TAMPERE UNIVERSITY OF TECHNOLOGY

FARAZ AHMED

DEVELOPMENTS IN POWER AMPLIFIER MODULE AND COMPARISON OF CIRCULATORS FOR SOLID-STATE MICROWAVE OVENS

Master of Science Thesis

Supervisor: Dr. Klaus Werner
Examiners: DrTech. Olli-Pekka Lunden
DrTech. Jari Kangas

Examiners and topic approved in the council meeting of Faculty of Computing and Electrical Engineering on March 6th, 2013.

ABSTRACT

TAMPERE UNIVERSITY OF TECHNOLOGY
Master's Degree Programme in Electrical Engineering
FARAZ AHMED: Developments in power amplifier module and comparison of circulators for solid-state microwave ovens.
Master of Science Thesis, 44 pages, 16 Appendix pages
March, 2013
Major: Radio Frequency Electronics
Supervisor: Dr. Klaus Werner
Examiners: DrTech. Olli-Pekka Lunden , DrTech. Jari Kangas
Keywords: ISM band, power amplifier, circulator, directional coupler, RF power detector

The solid-state microwave ovens (SSMO) use solid-state power amplifiers for heating food inside the oven cavity. These cooking devices are intelligent systems that can change RF signal characteristics in terms of power, frequency and signal phase. The solid-state transistors are rugged, smaller and cheaper than magnetrons. The SSMO is one step forward towards replacing the vacuum tube (magnetron) technology in heating applications such as microwave ovens.

This thesis presents the work done in the developments of power amplifier (PA) module designed for SSMO system. The PA module operates in industrial, scientific, and medical (ISM) band at 2.45 GHz with 250 W output power. Four PA modules are utilized in the SSMO system for multi-channel delivery of RF power into the oven cavity. The key achievements of this thesis are the analysis of faulty PA modules, characterization of RF power detector, and comparison of circulators.

Burnouts were observed in several 1^{st} generation PA modules. Failure analysis is made to thoroughly investigate the problem, and to find an enduring solution. RF power detector is developed to avoid burnouts in the future. The power detector monitors the flow of RF power from PA module to oven cavity. It gives the feedback to SSMO system in terms of forward and reflected RF powers. Moreover, five commercial circulators from five different suppliers are compared on identical test-fixtures. The comparison is based on electrical and thermal performance of each circulator as in test cases devised from the operation of the SSMO system.

PREFACE

Studying and working abroad are among the best experiences of my life so far. This gives me an opportunity to meet new people and get to know different cultures and traditions. At the same time, it helps me improve myself personally and professionally. I am so grateful to Allah the almighty for his utmost blessings and divine guidance. He gave me the strength to accomplish this task. I express my heartiest gratitude to the supervisor and the examiners for their continuous support, invaluable suggestions and advice during the whole process.

This thesis is an industrial development work being carried out during a 06 months traineeship in NXP Semiconductors, Nijmegen Netherlands. The same work is presented to pursue a Master of Science degree in Electrical Engineering offered by Tampere University of Technology, Tampere Finland. The external supervision is done by program manager Dr. Klaus Werner from High performance RF department at NXP. The thesis examination is done by DrTech. Olli-Pekka Lunden and DrTech. Jari kangas from Electronics department at TUT. I would also like to acknowledge the technical support by Andreas Koroulis, Victor Torres and Farhat Abbas from NXP, and for sharing their valuable experience with me.

I am so grateful to my parents and siblings for their continuous support and enduring love. I would also like to mention all my friends in Pakistan, Finland and Netherlands for making my life so exciting. I can hardly imagine my life without all of you. Finally, I dedicate this work to my deceased younger brother Maaz Ahmed R.I.P, who will always be missed.

AHMED FARAZ
Tampere, Finland
pharaxe@gmail.com
+358-50-4828151

CONTENTS

LIST OF ABBREVIATIONS

ACU	Acquisition and Control Unit
ADC	Analog to Digital Converter
BJT	Bipolar Junction Transistor
CCW	Counter Clockwise
CW	Clockwise
FET	Field-effect Transistor
GaAs	Gallium Arsenide
GaN	Gallium Nitride
HBT	Heterojunction Bipolar Transistor
HEMT	High Electron Mobility Transistor
I2C	Inter-Integrated Circuit
ISM	Industrial, Scientific, and Medical
JTAG	Joint Test Action Group
LDMOS	Laterally Diffused Metal Oxide Semiconductor
MESFET	Metal Semiconductor Field Effect Transistor
MOSFET	Metal Oxide Semiconductor Field Effect Transistor
NXP	Next Experience
OC	Open Circuit
PA	Power Amplifier
PSU	Power Supply Unit
RF	Radio Frequency
RL	Return Loss
SC	Short Circuit
Si	Silicon
SiC	Silicon Carbide
SPI	Serial Peripheral Interface
SSB	Small Signal Board
SSMO	Solid State Microwave Oven
TEM	Transverse ElectroMagnetic
UI	User Interface
VSWR	Voltage Standing Wave Ratio

LIST OF SYMBOLS

θ	Conduction angle
γ	Complex propagation constant
α	Attenuation constant
α_d	Attenuation due to dielectric loss
α_c	Attenuation due to conductor loss
β	Phase constant
ω	Angular frequency
Z_o	Characteristic impedance
k_o	Wave number in free space
ϵ_o	Free space permittivity
μ_o	Free space permeability
$\tan \delta$	Loss tangent
ϵ	Complex permittivity of the material
σ	Conductivity of the material
A	Thermal conductivity of the material
ΔT	Temperature rise
S_{11}	Input return loss, two-port network
S_{22}	Output return loss, two-port network
S_{21}	Insertion loss, two-port network
S_{12}	Isolation, two-port network

LIST OF FIGURES

LIST OF TABLES

1. INTRODUCTION

Today microwave ovens are commonly found in homes, shops, and workplaces. They are considered as an essential part of our daily life. Conventional microwave ovens are powered by magnetrons that generate microwave energy for heating food inside the oven cavity. The magnetron is essentially a vacuum tube which generates power by controlling current through two or more electrodes in an airtight enclosure. Vacuum tubes are known to be fragile, bulky and expensive. On the other hand, solid-state transistors are more rugged, smaller and cheaper than vacuum tubes. Solid-state devices have already replaced vacuum tubes in most applications such as amplifiers, switches, rectifiers, and radio broadcasting systems. Currently, research and developments are going on to exploit solid-state technology in heating applications. One such step forward is the solid-state microwave oven (SSMO) which uses solid-state power amplifiers for heating food inside the oven cavity. SSMO is a joint venture between NXP Semiconductors and other partner companies to introduce next generation cooking device in the market.

This chapter presents a brief overview of the SSMO system in section 1.1. Section 1.2 covers the power amplifier module designed for SSMO. It also highlights the issues with the current PA module. Lastly, section 1.3 highlights the main contributions of this thesis work in the development of SSMO project.

1.1 System overview

The SSMO system consists of an oven cavity, power amplifier (PA) module, power supply unit (PSU), and small signal board (SSB). It is an intelligent feedback system that can change frequency, power, and phase of the output signal according to the food inside the oven cavity. The heart of this device is a 250 W PA module. Four PA modules are present in the system delivering 1 kW RF power into the oven cavity. The SSMO operations and functions are controlled by a small-signal board which also carries cooking programs and recipes.

The oven cavity has a temperature sensor inside. It also has user interface (UI), and acquisition & control unit (ACU) on the front side. Four antennas are coupled to the bottom side of cavity for multi-channel RF power delivery. The SSB is further divided in three parts namely *SSB-Digital*, *SSB-RF* and *SSB-PSU*. SSB-Digital has a master microcontroller that communicates with SSB-RF and SSB-

PSU. The SSMO system receives the feedback from PSU and PA via I^2C Bus [1, p.3]. It also communicates with UI and ACU with a dedicated so called *Wide Bus*. The wide bus is not a standard communication protocol rather it is a company specific protocol. Communication between SSB-Digital and SSB-RF is through serial

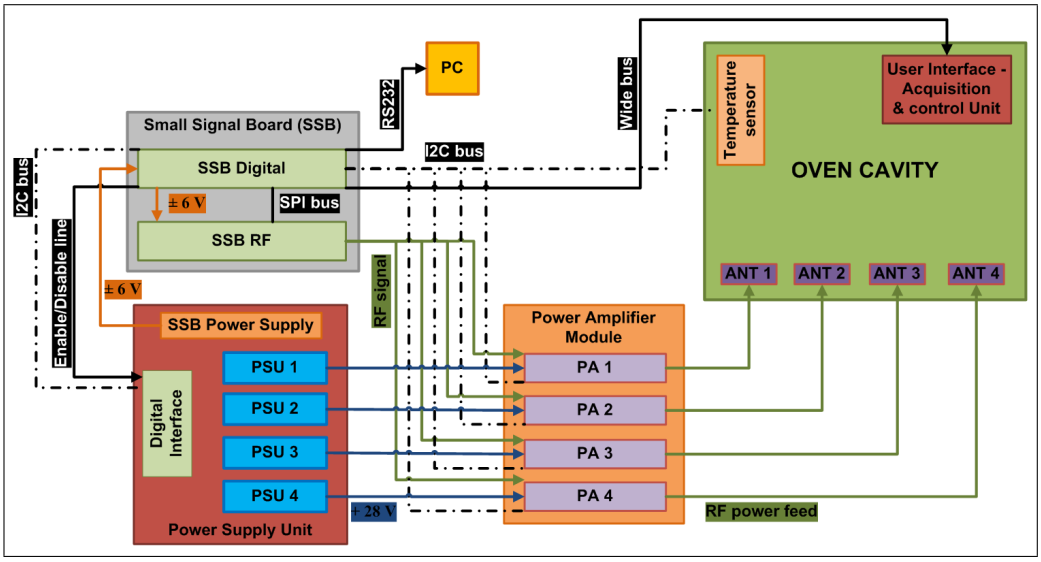

Figure 1.1: Block diagram of the system for solid state microwave oven

peripheral interface (SPI) Bus [1, p.2]. It also has standard test port called *JTAG* [2, 3] interface for testing and debugging the PCB. Figure 1.1 shows a simplified block diagram of the system.

1.2 Power amplifier module

Figure 1.2 presents the block diagram of a single PA module. It includes an amplifier,

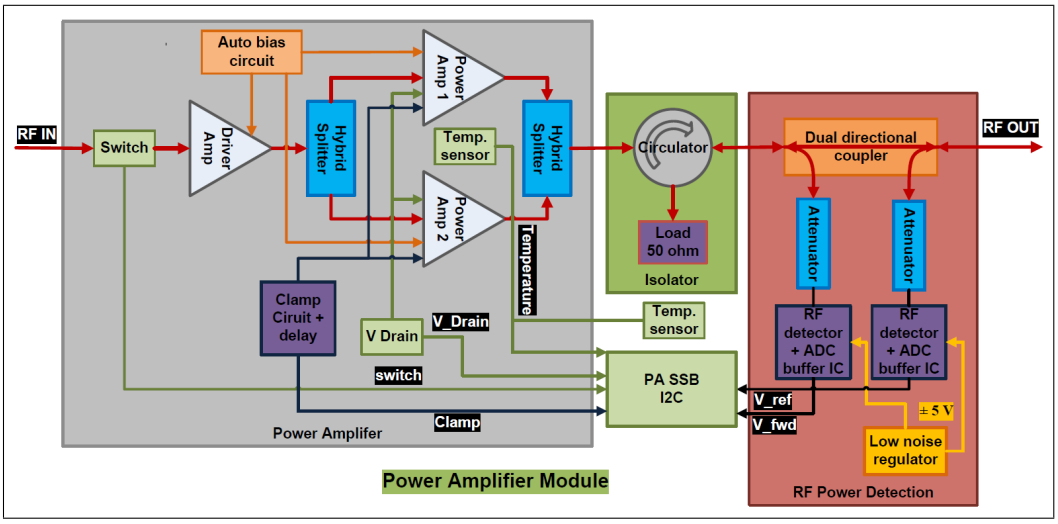

Figure 1.2: Block diagram of 1st generation PA module

an isolator, RF power detector and a small signal board called *PA-SSB*. Each power amplifier module is designed to operate in industrial, scientific and medical (ISM) band at 2.45 $\pm$ 0.05 GHz with nominal RF output power of 250 W. The transistor used in driver stage is *BLF25M612G*, and transistor used in power stage is *BLF2425M7LS250P*, respectively [4, 5].

Each PA module is mounted on a metal base plate for dissipating heat during its operation. The base plate has meander type water channels underneath. The base plates of all four PA modules are connected to a cooling bath which cools down the whole assembly. Isolator is used to protect the PA module from output reflections from the oven cavity. Power detector is used to monitor the forward power from PA module, and reflected power from the oven cavity respectively. PA-SSB is used to send real time feedback of measured parameters namely forward and reflected powers, module temperature, switch, and clamp state, and drain voltage from each PA module to main SSB.

Issues with the Power amplifier module

Being a graduate student of RF electronics, my work was solely focused on the power amplifier module. When I joined the RF team in Nijmegen we already had the prototypes for 1st generation PA module. However we have observed burnouts inside the number of modules. To proceed further in the developments, a systematic analysis of these faulty PAs and finding a lasting solution of the problem was thus essential. On the other hand a substantial effort was required for the selection of a suitable circulator for the 2nd generation PA module design.

1.3 Main contributions of the thesis

My key contributions are in the development of power amplifier module. In the 1st generation PA modules, I made a failure analysis and characterized the RF power detector. Moreover I made a comparison of circulators for the 2nd generation PA modules.

The failure analysis is based on Ishikawa approach [6]. This method is widely used in industries to analyze a fault systematically, and to find out the root cause of the failure. I analyzed the faulty PA modules for the burnouts observed at the output transmission line from the circulator to the antenna. Next I characterized the RF power detector for the output voltages in forward and reverse direction with respect to input power.

Five circulators from five different suppliers are compared as in certain test cases dictated by the application. The comparison of circulators is based on their thermal and electrical performance on identical test-fixtures. The key parameters for elec-

trical performance are isolation, insertion loss, and input output return losses from each test-fixture. Temperature rise in the output transmission line is measured as the thermal performance of each test-fixture.

Chapter 2 covers the theoretical background and formulates the necessary technical grounds for the reader. Chapter 3 presents the developments in the 1st generation PA modules. Chapter 4 presents the comparison of circulators for the 2nd generation PA modules, and the conclusion is made in chapter 5.

2. THEORETICAL BACKGROUND

This chapter presents the theoretical knowledge of power amplifiers, circulators and directional couplers. Moreover this chapter also covers the power measurement technique using directional coupler and basics of microstrip transmission lines. The discussion is started with a review on power amplifiers in section 2.1, classification of power amplifiers, and their performance parameters.

The basic concepts of circulators and directional couplers are discussed next in section 2.2 and section 2.3 respectively, including their theory of operation, and performance parameters. Power measurements using couplers are covered in section 2.4, microstrip transmission lines are covered in section 2.5, and a summary is presented at the end of the chapter.

2.1 Power amplifiers

The power amplifier is the basic building block in all wireless communication systems [7, 8], where it is used for signal amplification. The principle role of a power amplifier is to increase the signal power at its input up to a certain signal power at its output in a given frequency range [7, 8, 9, 10, 11].

The application area of power amplifiers is vast spanning from industrial, scientific and medical markets to wireless communication, broadcast, aerospace and defense [7, 8]. Power amplifiers are present in numerous electronic systems present today ranging from battery powered devices to medical imaging and satellite systems signify just a few examples [8]. Microwave heating is yet another industrial application where expedition is going on to exploit power amplifier inside microwave ovens.

Often the most expensive and the key component in a power amplifier is the active device or transistor used. Selection of a particular device technology is greatly dependent on the application and electronic system for which the amplifier is designed for. Figure 2.1 presents the power device technology tree [8, p.29]. Solid-state power devices can be grouped in two broad categories; Bipolar junction transistors (BJTs)

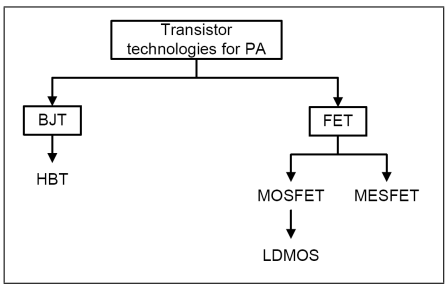

Figure 2.1: Transistor technologies for power amplifiers

and Field-effect transistors (FETs). Currently these devices are grown in silicon (Si), silicon carbide (SiC), gallium arsenide (GaAs), gallium nitride (GaN) and related compounds. Decades of search and exploration for semiconductor compounds suitable for high frequency operation lead to the development of improved structures [12, 13] such as Metal oxide semiconductor FET (MOSFETs), Metal semiconductor FET (MESFETs), Heterojunction BJT (HBTs), High electron mobility transistor (HEMT) and Laterally diffused MOSFET (LDMOS).

2.1.1 Classification of power amplifiers

Power amplifiers are categorized in terms of their class of operation. The traditional classes are referred as biasing class A, B, AB and C [8, 9, 10]. These classes are essentially derived from the active device's bias point selection in the design of a PA. There are present more classes of operation such as D, E, F and so on. However these are advanced classes and are derived from the dynamic operating conditions of the active device.

For instance, in current-mode the active device acts as a current source and in case of switched-mode the active device behaves as a switch. Figure 2.2 presents the power amplifiers classification structure [8, p.25]. Here we will discuss only the operation of biasing class A, B, AB and C in detail. For this purpose a rather convenient term conduction angle θ is defined [8, p.23] [14, p.355] which refers as the part of the input signal actually being amplified. In other words it is the portion of the input signal cycle during which transistor conducts. Table 2.1 presents some features for each biasing class [14, p.356]. For instance if a transistor remains 'ON' throughout the operation

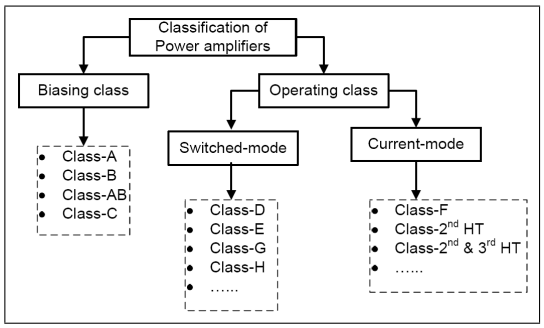

Figure 2.2: Power amplifier classificaiton

Table 2.1: Biasing classes of power amplifiers

Class of operation	conduction angle	Dependence on drive level	Quiescent point
A	$\theta = 360^o$	NO	Between cutoff and saturation
B	$\theta = 180^o$	NO	at cutoff
AB	$180^o < \theta < 360^o$	YES	above cutoff
C	$\theta < 180^o$	YES	below cutoff

and utilizes all the input signal for amplification then conduction angle is said to be 360^o. Likewise if a transistor remains 'ON' only for half time period of operation

and uses only half cycle of the input signal for amplification then conduction angle will be 180°.

2.1.2 Performance parameters of power amplifiers

The specifications and performance parameters of a power amplifier are closely connected to overall system requirements (especially in case of wireless communication systems), active device technology and operating conditions [7, 8]. However in most of the cases, the absolute output power level and power gain remains the prime performance metric for a PA.

Some requirements are in confrontation with one another for instance linearity and efficiency cannot be the best at the same time. Similarly, highest power output and least distortion cannot be achieved simultaneously. Thus PA design is always a compromise between various requirements and finding a best trade-off for a particular design. Nevertheless, efficiency, linearity and stability are the most challenging specification [8, p.27]. Listed below are various parameters and specifications for a power amplifier in general.

1. Output power (dBm)
2. Gain and gain flatness (dB)
3. Operating frequency and bandwidth (Hz)
4. DC supply requirements (V,I)
5. Input and output return loss (dB)
6. DC power consumption
7. Noise figure (dB)
8. Efficiency (%)
9. Linearity (1-dB compression)
10. Stability
11. Ruggedness
12. Heat management

2.2 Circulators

The circulators are essential building blocks of many electronic systems where they are used to protect or isolate different parts of circuits from one another from excessive signal reflections [15, 16, 17, 18, 19].

Two most common applications of the circulators are as duplexers and isolators [20]. For instance, duplexers are widely found in transceiver systems where they are used to couple single antenna to both the transmitter and the receiver system. Isolators are used as protection from unwanted reflected power or harmful reflections in a signal chain, for instance protecting a power amplifier from bad VSWR at the output.

2.2.1 Theory of operation

A circulator is a non-reciprocal passive device based on ferrimagnetic ceramic materials [21]. Theoretically circulators can have many ports. However, the most widely used devices today are the three-port Y-junction ferrite circulators. The non-reciprocity of the device is achieved by exploiting the magnetic properties of ferrite [22, 23, 24].

The principle operation of circulators is to permit the energy flow between two adjacent ports and in only one direction (Forward) while preventing the flow of energy in reverse direction. The flow of energy can be either clockwise (CW) or counter-clockwise (CCW). An ideal circulator is a lossless device having no insertion loss, no reflections at its ports and infinite isolation in the reverse direction of energy flow [25, p.535].

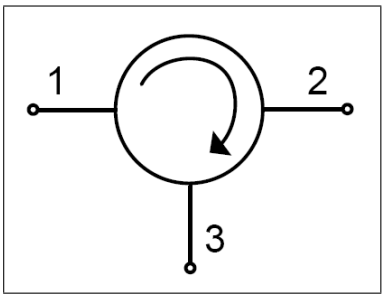

Figure 2.3: A Three-port circulator

Figure 2.3 presents the symbol of a three-port CW circulator. In such circulator the energy could flow from port 1 to port 2, from port 2 to port 3 or from port 3 to port 1 in forward direction with some insertion loss. On the contrary such circulator prevents the flow of energy from port 2 to port 1, from port 3 to port 2 and from port 1 to port 3 with significant isolation.

Scattering matrix

An ideal three-port circultor can be defined in terms of scattering matrix [25, 19, 26] which is given by

$$\begin{bmatrix} P_1' \\ P_2' \\ P_3' \end{bmatrix} = \begin{bmatrix} S_{11} & S_{12} & S_{13} \\ S_{21} & S_{22} & S_{23} \\ S_{31} & S_{32} & S_{33} \end{bmatrix} \begin{bmatrix} P_1 \\ P_2 \\ P_3 \end{bmatrix} , \tag{2.1}$$

where P_i and P_i' denotes the input and output power at corresponding port, respectively. For a lossless circulator equation (2.2), and for perfectly matched ports equation (2.3) must hold as

$$[S]^*[S] = 1 , \tag{2.2}$$

$$S_{11} = S_{22} = S_{33} = 0 . \tag{2.3}$$

By means of the unitary properties of scattering matrix we can demonstrate that such a device must be nonreciprocal by nature that is $S_{ij} \neq S_{ji}$. The resulting

scattering matrix is given by

$$[\mathrm{S}_{\text{ideal CW}}] = \begin{bmatrix} 0 & 0 & 1 \\ 1 & 0 & 0 \\ 0 & 1 & 0 \end{bmatrix}, \tag{2.4}$$

which shows that power will flow only from port 1 to 2, 2 to 3, and 3 to 1 [25, p.476]. Rotation in such a case is said to be clockwise (CW). Likewise if we transpose the port indices, counter-clockwise (CCW) rotation can be achieved.

Now consider the scattering matrix [25, p.477] of a circulator which is not perfectly matched. It has small reflections $\Gamma << 1$, and a circular symmetry (non-reciprocity) of $\mathrm{S_{ij}} \neq S_{ji}$. Parameter β is the isolation constant and parameter α is the transmission constant, respectively. Assuming that the circulator is lossless and ignoring the phase factors it can be proved [25] that the isolation equals to $\beta \simeq \Gamma$, and transmission equals to $\alpha \simeq 1 - \Gamma^2$. For such a circulator the scattering matrix is given by

$$[\mathrm{S}_{\text{real}}] = \begin{bmatrix} \Gamma & \beta & \alpha \\ \alpha & \Gamma & \beta \\ \beta & \alpha & \Gamma \end{bmatrix} \begin{bmatrix} \Gamma & \Gamma & 1-\Gamma^2 \\ 1-\Gamma^2 & \Gamma & \Gamma \\ \Gamma & 1-\Gamma^2 & \Gamma \end{bmatrix}, \tag{2.5}$$

which implies that the isolation of this circulator is approximately equal to the reflections or return loss at the input ports. Both isolation and insertion loss degrades as the mismatch increases.

2.2.2 Performance parameters

Consider a circulator as depicted in figure 2.4 having CW rotation with its input as port 1, output as port 2 while port 3 is terminated with a matched load, consequently converting it into an isolator. The key performance parameters of such circulators are isolation, insertion loss, VSWR or Return loss (RL) and power capacity [20, 27].

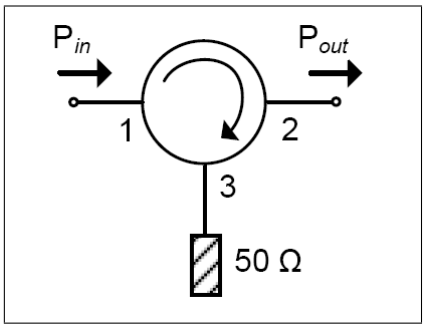

Figure 2.4: Three-port circulator as an isolator

Insertion loss

Insertion loss describes the attenuation to the input signal from one port to another in forward direction and it is expressed in decibels. The higher the insertion loss the more power is dissipated in the circulator and converted into heat. From figure 2.4

insertion loss is given by

$$\text{Insertion} = 10\log_{10}\left(\frac{\mathrm{P_{in}}}{\mathrm{P_{out}}}\right)\ [dB]\ . \tag{2.6}$$

Isolation

Isolation is the most important performance parameter of an isolator. It defines how fine the power coming from the output port is prevented from reflecting back into the input port. Or in other words how much the input port is protected against the output port in reverse direction. From figure 2.4 isolation is given by

$$\text{Isolation} = 10\log_{10}\left(\frac{\mathrm{P_{out}}}{\mathrm{P_{in}}}\right)\ [dB]\ . \tag{2.7}$$

It should be worthy to understand that the load termination attached to port 3 plays a critical role in defining the degree of isolation. A superior quality of the load and excellent VSWR at port 3 leads to better isolation. Consider the following example to better understand the operation of a lossless circulator.

Example 1: A lossless circulator is connected to 50 ohm load at port 3, resulting in an isolation of 20 dB from port 1 to port 2. A 250 W input power is fed to port 1, and port 2 is made perfect open circuit (OC). Neglecting the transmission line losses, and assuming perfect match at port 3, calculate how much power in percentage is reflected back to the input.
Answer: Insertion loss = 0 dB, Isolation = 20 dB, $\mathrm{P_{in}}$ = 250 W $\approx$ 54dBm.
$\mathrm{P_{ref}}$ = 54 dBm $-$ 20 dB = 34 dBm $\approx$ 2.5 W.
% of $\mathrm{P_{ref}}$ = 2.5 W/250 W x100 = 1 %.
1 % of the power will reflect back from port 2 to port 1. However, rest of the power will absorb in the 50 ohm load termination.

2.3 Directional couplers

Couplers are multi-port passive microwave devices that are used to extract small amount of power from the main transmission line to a coupled port [25, 15, 19, 18, 16]. Couplers can be grouped in to two broad categories; waveguide couplers and microstrip couplers. Waveguide couplers include Bethe-hole coupler, multi-hole coupler, and Schwinger coupler while microstrip couplers include coupled-line coupler, branch-line coupler and Lange coupler [25, 19]. Couplers can have three

ports or four ports, however four-port directional coupler are conceivably the most widely used couplers today and are covered in more details here.

Directional couplers have found their applications in various commercial and military electronic systems [28, 29], where they are commonly used for power flow monitoring, signal sampling, and measuring forward and reverse waves for determining a mismatch. Moreover 3-dB directional couplers can be used as power dividers. They are also commonly found in many microwave mixers and in balanced amplifiers [19, p.413]. For instance a military radar system with transmitter at port 1, antenna at port 2, a detector at port 3 and matched load at port 4 is a classic example of power monitoring.

2.3.1 Theory of operation

The basic working principle of a coupled-line microstrip directional coupler is to extract power from a main transmission line to another transmission line present in its close proximity. An ideal coupler is a lossless device with all its ports perfectly matched. As depicted in the figure 2.5, wave incident in port 1 (input) will travel through port 2 (through) while certain amount of incident wave will couple in to port 3 (coupled) and no wave will travel through port 4 (isolated).

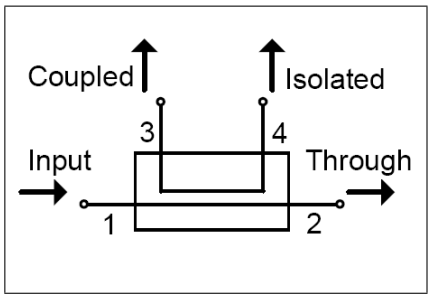

Figure 2.5: A Four-port directional coupler

Scattering matrix

The scattering matrix of four-port directional coupler is given by

$$\begin{bmatrix} b_1 \\ b_2 \\ b_3 \\ b_4 \end{bmatrix} = \begin{bmatrix} S_{11} & S_{12} & S_{13} & S_{14} \\ S_{21} & S_{22} & S_{23} & S_{24} \\ S_{31} & S_{32} & S_{33} & S_{34} \\ S_{41} & S_{42} & S_{43} & S_{44} \end{bmatrix} \begin{bmatrix} a_1 \\ a_2 \\ a_3 \\ a_4 \end{bmatrix}, \tag{2.8}$$

where a_i and b_i are the incident and reflected waves at port i. Assuming all the ports to be perfectly matched, equation (2.9) must hold. Moreover assuming perfect isolation from port 1 to 4, and from port 2 to 3, equation (2.10) must hold true.

$$\mathrm{S}_{11} = \mathrm{S}_{22} = \mathrm{S}_{33} = \mathrm{S}_{44} = 0 \tag{2.9}$$

$$\mathrm{S}_{14} = \mathrm{S}_{23} = 0 \tag{2.10}$$

Further assuming all the coupling elements to be non-zero and using the symmetry

and unitary properties [25, p.354], the scattering matrix is reduced to

$$[\mathrm{S}] = \begin{bmatrix} 0 & S_{12} & S_{13} & 0 \\ S_{21} & 0 & 0 & S_{24} \\ S_{31} & 0 & 0 & S_{34} \\ 0 & S_{42} & S_{43} & 0 \end{bmatrix} = \begin{bmatrix} 0 & \alpha & \beta & 0 \\ \alpha & 0 & 0 & -\beta \\ \beta & 0 & 0 & \alpha \\ 0 & -\beta & \alpha & 0 \end{bmatrix}, \tag{2.11}$$

where amplitudes α and β are related as $\alpha^2 + \beta^2 = 1$.

2.3.2 Performance parameters

The key performance parameters for directional couplers are coupling, isolation, directivity and insertion loss. These parameters can be defined using [S] matrix from equation (2.11).

Coupling

Coupling ratio is defined as the nominal level of the input signal at the coupled port. Typical values for coupling are 10, 20 and 30 dB, and is given by

$$\text{Coupling, } \mathrm{C} = 10\log_{10}\left(\frac{\mathrm{P_{input}}}{\mathrm{P_{coupled}}}\right) = -20\log_{10}\beta \ \ [dB]\,. \tag{2.12}$$

Isolation

Isolation is defined as the nominal level of the input signal at isolated port when port 2 is terminated with a matched load. Isolation is given by

$$\text{Isolation, } \mathrm{I} = 10\log_{10}\left(\frac{\mathrm{P_{input}}}{\mathrm{P_{isolated}}}\right) = -20\log_{10}|\mathrm{S_{14}}| \ \ [dB]\,. \tag{2.13}$$

Directivity

Directivity is defined as the ability of the coupler to distinguish between forward and reverse waves. In other words how well the incident and reflected waves are isolated from one another. High directivity of a coupler is always desirable, and it can be expressed as

$$\text{Directivity, } \mathrm{D} = \mathrm{I} - \mathrm{C} = 10\log_{10}\left(\frac{\mathrm{P_{coupled}}}{\mathrm{P_{isolated}}}\right) = 20\log_{10}\frac{\beta}{|\mathrm{S_{14}}|} \ \ [dB]\,. \tag{2.14}$$

Insertion loss

Insertion loss is described as the attenuation to the input signal in the main transmission line while traveling through port 1 to port 2. It also includes the signal loss

due to coupling. Typical values for insertion loss are from 0.2 to 0.5 dB, and it can be written as

$$\text{Insertionloss, } \mathrm{L_{main}} = 10\log_{10}\left(\frac{\mathrm{P_{input}}}{\mathrm{P_{output}}}\right) = -20\log_{10}\alpha \;\; [dB]\;. \tag{2.15}$$

2.4 Power measurements using couplers

One widely used method of making high power measurements is to use directional couplers, power sensors and power meters [30, 31, 32]. The basic idea is to tap small portion of RF signal from the main power line. Among many manufacturers Agilent has developed wide range of meters and sensors [33] for RF and microwave power measurements. Figure 2.6 presents a generic test bench for power measurement of a high power amplifier.

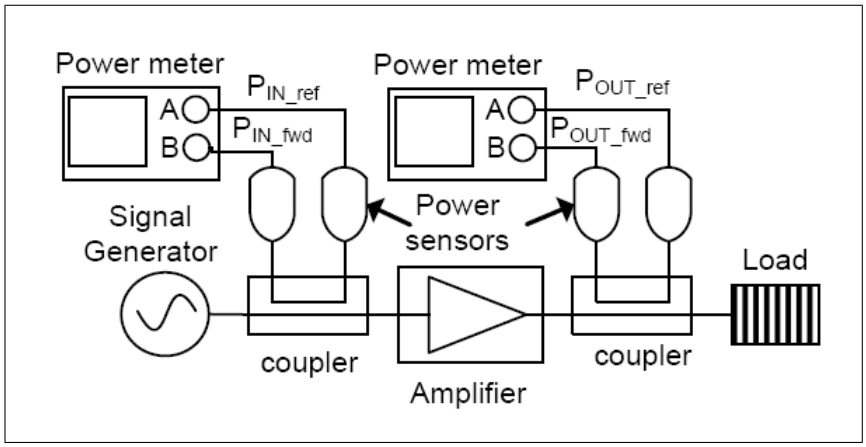

Figure 2.6: Generic test bench for power measurements

In the figure the device under test (DUT) or the amplifier is connected to a signal generator at its input and to a load at its output. Similarly two directional couplers are placed in between the input and the output of the amplifier and sensors are connected to both coupled and isolated ports of these directional couplers.

Power available from the generator is measured as $\mathrm{P_{IN,fwd}}$ from the coupled port and power reflected back from the input of the amplifier due to mismatch is measured as $\mathrm{P_{IN,ref}}$ from the isolated port of the coupler. Similarly power delivered to the load is measured as $\mathrm{P_{OUT,fwd}}$ from the coupled port and power reflected back from the load due to mismatch is measured as $\mathrm{P_{OUT,ref}}$ from the isolated port of the coupler.

Measurement accuracy

Measurement accuracy depends upon many factors including instrument calibration, sensor accuracy and directivity of the coupler. Conceivably the first factor to consider is to achieve a fine calibration of the power meter. Calibration usually involves

setting up the instrument to a predefined reference set of measurements values. Sensors are important because they can easily be overloaded and operated beyond their normal range of operations. Normally sensors have wide dynamic ranges however care must be taken to make sure that they remain in their nominal operating range.

Directivity errors and measurement uncertainties

As already explained before, directivity of a coupler is its ability to distinguish between forward and reverse travelling waves. A perfect coupler has infinite isolation while real couplers have finite isolation, which means that some power will always be detected at the isolated port even in a perfect match condition, this is known as directivity error which produce uncertainties in the measurements.

In forward power $P_{IN,fwd}$ and $P_{OUT,fwd}$ measurements at the coupled ports, the detected signal is the vector sum of two waves; the wanted forward coupled waves and the unwanted or leaked reverse waves. These two waves add with arbitrary phase. Likewise in reverse power $P_{IN,ref}$ and $P_{OUT,ref}$ measurements at the isolated ports, the detected signal is also the vector sum of two waves; the wanted reverse coupled waves (typically much lower) and the unwanted or leaked forward waves (typically much higher). These measurements are more challenging because coupler has to distinguish a lower amplitude reflected wave over an undesired leaked forward wave of much higher amplitude.

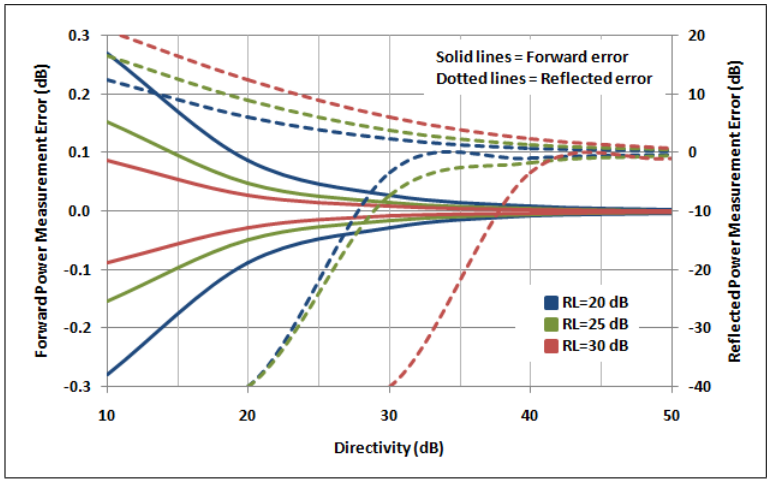

Figure 2.7: Directivity errors and measurement uncertainties

Figure 2.7 presents the theoretical measurement uncertainties related to directivity errors [34]. Both forward power error and reflected power error graphs are plotted on left and right hand side of the vertical axis with respect to directivity on the horizontal axis. All the values are plotted in decibel scale. Three mismatch cases are treated having return losses of 20 dB, 25 dB and 30 dB. It should be noted that in case of forward power measurements; 20 dB of directivity has ± 0.1 dB of

error, on the contrary the same directivity has +12, −40 dB of error in reverse power measurements. However a directivity of 50 dB has ±0.1 dB of error in the reverse power measurements. This suggest us that reverse power measurements are highly sensitive and demands higher directivities.

2.5 Microstrip transmission lines

Figure 2.8 presents the lumped-element circuit model for a two-wire transmission line [25, p.50]. Parameters R and G represent losses due to the resistance of the conductor, and the dielectric loss of the material between the conductors respectively. Moreover, parameters L and C present the self-inductance and the shunt capacitance of the two conductors, respectively. In such a network voltage v and current i vary its magnitude and phase over the infinitesimal length Δz of the transmission line. By applying Kirchhoff's voltage and current laws for this lumped network and taking a dividend of Δz results in differential equations presented in [25], which are the time-domain representation of the telegrapher equations

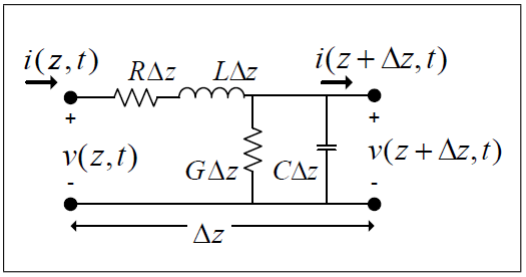

Figure 2.8: Transmission line model

$$\frac{dV(z)}{dz} = -(R + j\omega L)\, I(z)\,, \tag{2.16a}$$

$$\frac{dI(z)}{dz} = -(G + j\omega C)\, V(z)\,. \tag{2.16b}$$

These equations can be solved simultaneously for $V(z)$ and $I(z)$, and for defining the wave propagation constant and the characteristic impedance of the transmission line. The complex propagation constant γ can be defined as

$$\gamma \;=\; \alpha + j\beta \;=\; \sqrt{(R + j\omega L)(G + j\omega C)}\,, \tag{2.17}$$

where α is the attenuation constant and β is the phase constant. Similarly, the characteristic impedance Z_o can be defined as

$$Z_o \;=\; \frac{R + j\omega L}{\gamma} \;=\; \sqrt{\frac{R + j\omega L}{G + j\omega C}}\,. \tag{2.18}$$

In a lossless transmission line ($R = G = 0$), equation (2.17) reduce to $\gamma = \alpha + j\beta = j\omega\sqrt{LC}$, where $\alpha = 0$ and $\beta = \omega\sqrt{LC}$. Similarly, equation (2.18) reduce to $Z_o = \sqrt{L/C}$.

In practice transmission lines have different forms of losses including conductor

loss, dielectric loss, radiation loss, and coupling loss [25, 19]. The additive effect of all these losses translates as the total loss in a transmission line. However, at microwave frequencies conductor loss and dielectric loss are imperative and require attention.

The *conductor loss* sometimes also called resistive heating is due to the fact that the conductor in a transmission line has finite conductivity. The flow of current through it causes heating due to resistance, and consequently raises temperature which results in power loss. On the other hand, the *dielectric loss* also called dielectric heating is due to the fact that material in between the two conductors has small conductance. A small amount of power is also dissipated in to the dielectric material which results in the heating of the dielectric and consequently the loss of power.

Microstrip

A microstrip is composed of a thin metal conductor and a ground plane separated by a dielectric material [25, p.143] [35, 36, 37]. Consider a strip conductor of width W on a grounded dielectric substrate of thickness H and relative permittivity ϵ_r. The effective dielectric constant ϵ_e and characteristic impedance Z_o of such microstrip transmission line are given by

$$\epsilon_e = \frac{\epsilon_r + 1}{2} + \frac{\epsilon_r - 1}{2} \frac{1}{\sqrt{1 + 12H/W}} , \tag{2.19}$$

$$Z_o = \begin{cases} \dfrac{60}{\sqrt{\epsilon_e}} ln\left(\dfrac{8H}{W} + \dfrac{W}{4H}\right) & \text{for } W/H \leq 1 , \\ \dfrac{120\pi}{\sqrt{\epsilon_e}[W/H + 1.393 + 0.667\, ln(W/H + 1.444)]} & \text{for } W/H \geq 1 . \end{cases} \tag{2.20}$$

The propagating mode along the strip conductor is not purely transverse electromagnetic (TEM) because the field lines between the conductor and the ground are not entirely confined inside the dielectric substrate. In order to estimate the losses, the microstrip is treated as quasi-TEM transmission line and the attenuation due to dielectric loss is given by

$$\alpha_d = \frac{k_o \epsilon_r (\epsilon_e - 1) \tan \delta}{2\sqrt{\epsilon_e}(\epsilon_r - 1)} \quad [Np/m] , \tag{2.21}$$

where $k_o = \omega\sqrt{\mu_o \epsilon_o}$ is the wave number in free space, and $\tan \delta = \epsilon^{''}/\epsilon^{'}$ is the loss tangent of the dielectric material defined in terms of complex permittivity $\epsilon = \epsilon^{'} - j\epsilon^{''}$. The real permittivity of the material is defined as $\epsilon^{'} = \epsilon_o \epsilon_r$. Considering the fact that field distributions of a microstrip line are partly inside the dielectric material and partly in the air, a *filling factor*$= \epsilon_r(\epsilon_e - 1)/\epsilon_e(\epsilon_r - 1)$ is also introduced.

The attenuation due to the conductor loss is given by

$$\alpha_c = \frac{R_s}{Z_o W} \quad [Np/m] \,, \tag{2.22}$$

where sheet resistance R_s is given by $R_s = \sqrt{\omega\mu_o/2\sigma}$. Here μ_o is the free space permeability and σ is the conductivity of the microstrip material. It should be noted that this expression gives an approximation assuming uniform current distributions across the width of the conductor and ground plane. Now the total attenuation constant due to conductor loss and dielectric loss is $\alpha = \alpha_c + \alpha_d$, and $\alpha(dB) = 20\ log\ e^{2\alpha}$ in decibel per unit length.

Resistive heating and temperature rise

Figure 2.9 presents the microstrip model with a conductor of length L, and width W. The dielectric substrate has thickness H, dielectric constant ϵ_r and thermal conductivity A.

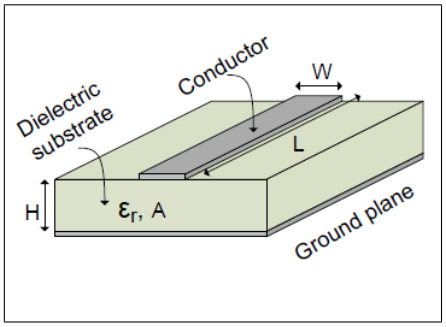

Figure 2.9: Microstrip model

The temperature rise ΔT of the microstrip conductor due to incident RF power P_I is determined by various factors including transmission line losses, thermal conductivity of the substrate, surface area of the conductor, and ambient temperature. Consequently, the power handling capability of a microstrip is limited by the resistive heating of the conductor, the dielectric heating of the substrate, and by the dielectric breakdown [38].

A straight-forward approach is presented in [39] for the estimation of temperature rise and the calculation of RF resistive heating of a microstrip conductor. However this approach provides a rather conservative and simple estimate based on the following assumptions,

- A steady state situation and perfect match (no reflections) conditions at the terminations are achieved.
- All the heat generated is apparent as temperature rise in the conductor trace, and the ground plane maintains a uniform temperature.
- All the loss of RF power is accounted as the heat generated in the conductor trace, neglecting radiation loss and heat dissipation in dielectric substrate.
- All the heat generated by the RF power is conducted along the length of the conductor trace to the ground, neglecting the fringing effects at the edges of

the conductor and neglecting heat carried away by the terminations at the ends.

The resistive heating due to RF power in a microstrip conductor can be estimated as

$$\Delta T \;=\; \frac{H P_I [1 - 10^{-ML/10}]}{L\, W\, A} \quad [^oC]\,, \tag{2.23}$$

where P_I is the incident power in watt, H is the dielectric thickness in meter, and A is the thermal conductivity of the dielectric in watt per Kelvin meter. M is the insertion loss in decibel per unit length, L is the length in meter and W is the width in meter, of the conductor trace, respectively. Consider the following example for estimating the temperature rise in a real PCB.

Example 2: Calculate the temperature rise in a microstrip conductor of *Rogers R*04350 *LoPro* PCB, due to incident RF power P_I of (a) 150 W and (b) 250 W. The substrate thickness of the PCB is H = 0.779 mm, and the dielectric constant is $\epsilon_r = 3.55$. It has thermal conductivity of A = 0.62 W/Km, and the insertion loss per unit length is M = 2.22262 dB/m. The length and width of the conductor is L = 8 mm and W = 1.71409 mm, respectively.
Answer: Using equation (2.23)

$$\Delta T \;=\; \frac{(0.779\ mm)(150\ W)[1 - 10^{(\frac{-(2.22262\ dB/m)(8\ mm)}{10})}]}{(8\ mm)\ (1.71409\ mm)\ (0.62\ W/mK)} \quad [^oC]\,.$$

(a) Temperature rise of ΔT = 56.27 °C is estimated for an incident power of P_I = 150 W.
(b) Temperature rise of ΔT = 93.78 °C is estimated for an incident power of P_I = 250 W.

It should be noted that these calculations are based on the assumptions mentioned before and yield an approximate solution. In practice the observed temperature rise could be higher.

2.6 Summary

Power amplifier is used for signal amplification in various electronic and communication systems. Traditionally they are categorized in classes namely A, B, AB, and C, which are derived from bias point selection of the active device. The key performance parameters of a power amplifier are its output power, gain, efficiency, stability, linearity and ruggedness.

Circulators are used to isolate different parts of electronic system from one another from unwanted signal reflections. A three-port circulator is a non-reciprocal passive

device based on ferrite material. The non-reciprocity of the device is achieved by exploiting the magnetic properties of the ferrite.

A four-port directional coupler is used to extract small amount of power from the main line to a coupled port where it is used for power flow monitoring and signal sampling. The key performance parameters of a coupler are its coupling factor, isolation from the main line, and directivity. Directivity plays a key role in power measurements using couplers and adds uncertainties in the measurements. Moreover reverse power measurements are more challenging as compared to forward power measurements.

The propagation mode along the strip conductor is not purely TEM, however they can be treated as qusai-TEM transmission lines. The proposed temperature rise calculations in a microstrip conductor due to resistive heating are rather simple. They give a conservative approximation of the actual measurement data.

3. DEVELOPMENTS IN POWER AMPLIFIER MODULE

In the 1st generation PA modules an antenna was integrated inside of each module. However during the normal operation of the PAs, burnouts were observed in several modules. The output transmission line from the circulator to the antenna burned out in number of occasions. Initially the problem was avoided by replacing the output transmission line with a small piece of rugged coaxial cable. Nonetheless, the issue prevails and in later cases the output lead of the circulator evaporates resulting in permanent damage to the circulator. Consequently, the team decided to thoroughly investigate the problem, and to find an enduring solution.

For this purpose I started with the analysis of faulty PA modules using Ishikawa method. I made a fishbone diagram corresponding to the burnouts. Next I list down all the possible causes that could contribute to such a failure, and speculate the root cause of the problem. Moreover, the team proposed a power detector to avoid burnouts in the future. This power detector monitors the flow of RF power from the PA module to the oven cavity, and gives real time feedback to the SSMO system. As a result, the system can decrease the input power in case of high reflected power from the oven cavity. A standalone prototype of such RF power detector was realized for later integration inside the PA modules. I made the characterization of the power detector. Consequently, assisting the team with the development in the 1st generation PA modules.

Section 3.1 covers the analysis of faulty PA modules using Ishikawa diagrams. Section 3.2 covers the RF power detector and its characterization, and a summary is presented at the end of the chapter.

3.1 Analysis of faulty PA modules

Ishikawa diagrams also referred as cause-and-effect or fishbone diagrams were first introduced by Ishikawa K. in 1960s [40]. Today this method is commonly used in industries to analyze a fault systematically. It enables graphical visualization of all the possible causes of a particular problem and investigates the true cause of the problem.

Failure analysis using Ishikawa approach is a four step process. In the first step we have to identify the problem in hand. Traditionally, the problem statement is en-

closed in a box on the right side of a bold horizontal line. Next step is to describe the key factors or categories that may contribute to the problem and draw each of them as spines or bones. Third step is to write down all the possible causes and sub-causes in each category. The fourth step is to analyze the diagram and speculate the root cause. Figure 3.1 presents the magnified snapshot of the faulty area of a PA module. The burned out trace and damaged circulator can be clearly seen from this figure. In order to graphically analyze this problem through fishbone diagram, we defined four distinct categories namely materials, design, manufacturing, and methods. Figure 3.2 presents the finalized fishbone diagram of the failure. In each category we brainstorm and list down all the possible causes that could contribute to such a failure. Subsequently we investigate in detail all the possible causes through factual

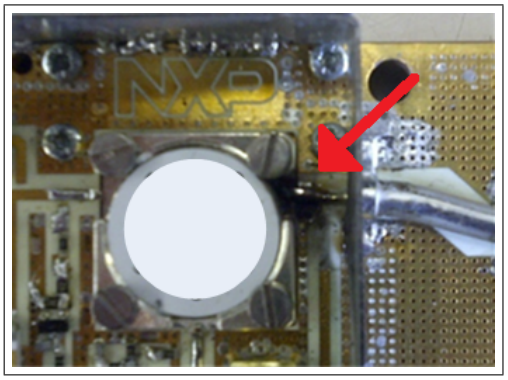

Figure 3.1: Faulty PA module

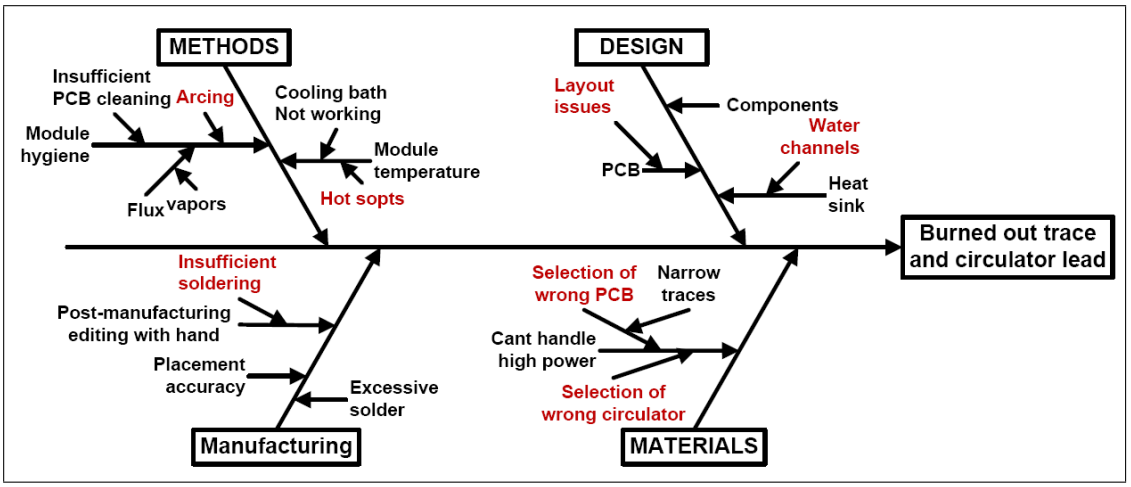

Figure 3.2: Failure analysis using fishbone diagram

reasoning and experiments, and at the end speculate the potential root cause.

3.1.1 Methods

This category defines the day-to-day practices during the operation of PA modules. For instance module hygiene and module temperature can be questioned as the potential cause of the failed devices. Although surrounding environment could contribute in this failure however we can neglect external agents and factors because all the modules are well shielded.

We inspected the faulty PA modules for improper cleaning. Unwanted intruders such as moist or flux could produce vapors during operation and can lead to electrical

arching. As standardized practice all electronic circuits should be properly cleaned from unwanted manufacturing remains, environment dust and moist prior to their operation. We followed the same practice hence this cause can be ruled out assuming that each PA module was properly cleaned before its operation.

There was always a cooling bath attached to the module during its operation. The metal base plate of the module contains meander type water channels underneath to cool down the whole PA assembly. Therefore we expect the overall temperature of the module to be 20 ^{o}C. However temperature rise above the temperature of base plate in RF traces could be higher due to high power flow, particularly at the output trace causing an increase in overall temperature of the PCB traces.

3.1.2 Manufacturing

In standardized practices electronic circuits are manufactured with precision to achieve desired performance. A good design could be ruined by minor manufacturing issues. Therefore care must be taken in manufacturing and this process must comply with the known industry standard practices.

In the 1st generation PA modules we have done post-manufacturing changes on the PCB. We have replaced the output trace with a piece of coaxial cable to avoid potential failure rather than examining the root cause. It did help us in short terms however in long terms this will never work because post-manufacturing changes by hands always have random effects and the overall performance varies per unit. Therefore this cause cannot be ruled out.

3.1.3 Design

In this category we questioned the design aspects of the PA modules as the potential cause of the failure. This is far more intricate since we have to look in to the details of PCB, components, heat sink (metal base plate), layout and so forth.

A common opinion about PCBs is that they cannot handle high powers at radio and microwave frequencies. However the selection of right PCB and modeling of right trace dimensions can promise medium powers. Normally PCB manufacturers provide a list of parameters from which one could speculate its performance in desired conditions. However power handling capabilities of these PCBs are dependent upon the application in which they are being used because trace width is a function of application frequency. On the other hand, keeping the operating temperature of the electronic devices controlled by means of cooling baths or heat sinks is a common practice.

In our design we have used R04350 PCB from Rogers Corporation [41]. The width of RF traces is 1.1 mm at 2.45 $\pm$ 0.05 GHz, which are subject to 250 W RF

power. A cooling bath is attached to the metal base plate of the module, which maintains a constant temperature of 20 ^{o}C. These conditions are favorites for the systems operating at high powers and temperatures, which suggest us that design aspects are not likely the root cause of this failure. Hence we can rule out these causes.

3.1.4 Materials

This category defines the potential materials responsible for the failure, and the most critical are PCB and circulator. Because the output lead of the circulator totally evaporates, this raises a question mark on the circulator itself.

Consequently we decided to experiment with the same PCB and circulator on a test-fixture as standalone unit. We performed two tests to investigate the ruggedness of the circulator to ensure that it is good enough to withstand all the worst conditions.

Lead stress test

In this test the circulator output lead is physically disconnected from the PCB with the help of kapton tape as depicted in Figure 3.3(a). In this manner we stressed the output lead independently from the contribution of the heat sink. This situation also means that the output lead is now in open circuit condition and has maximum

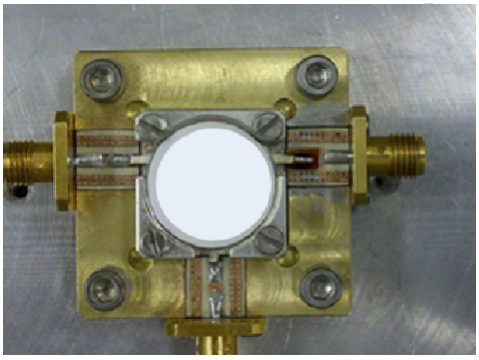

(a) Lead is physically isolated by kapton tape.

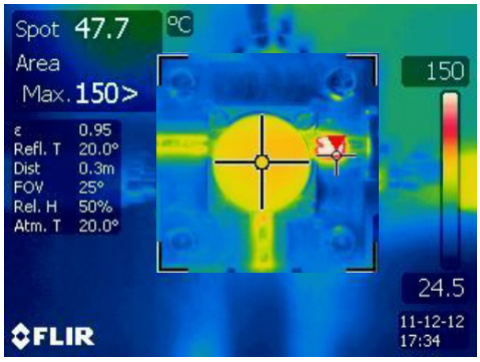

(b) Measured temperature at the output lead

Figure 3.3: Circulator lead stress test (a) Test-fixture snapshot, (b) Thermal image

reflections. Next we inject 250 W power to the circulator and after 15 minutes we took thermal reading at the output lead. No damage was seen at the lead and a temperature of more than 150 °C was measured as presented in Figure 3.3(b). The lead did not evaporate and no burnouts were observed after the test.

Reflections test

Then we stressed the circulator for highest possible reflections from the load with its output lead properly soldered on the PCB trace. For this purpose we utilized smith chart approach and take four points for the test namely open, short, inductive, and capacitive.

Figure 3.4 comprehend voltage and current phases at these conditions and their respective points on the smith chart. Next we took a slug tuner and characterize

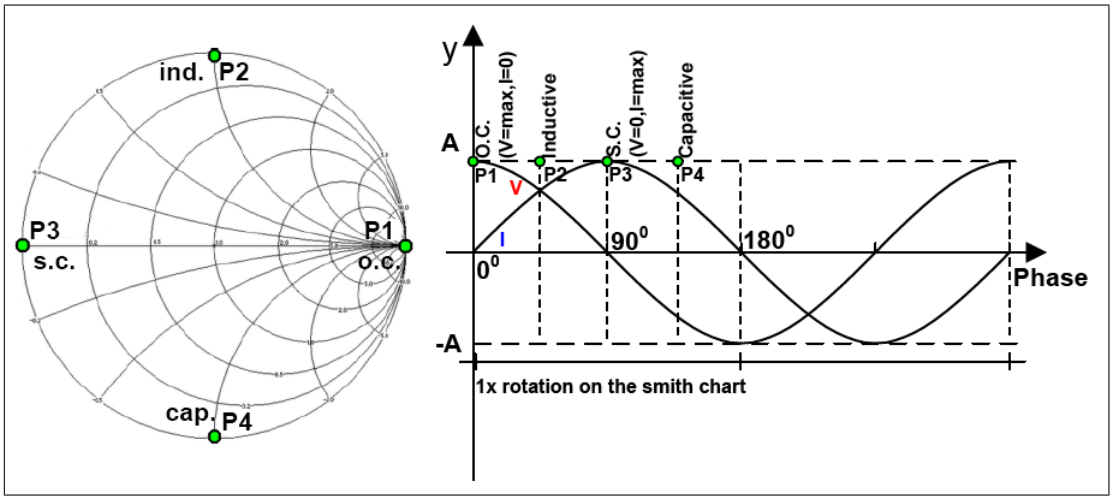

Figure 3.4: Current and voltage phases and smith chart

it with the network analyzer. We utilized the port extension technique to precisely achieve these four test points at the output lead of the circulator inside the test fixture. We measured the temperature at the very output lead of the circulator for each test points. The slug tuner is capable of handling 100 W power, so we extrapolated the measurement data up to 250 W. Figure 3.5 presents the reflections test results.

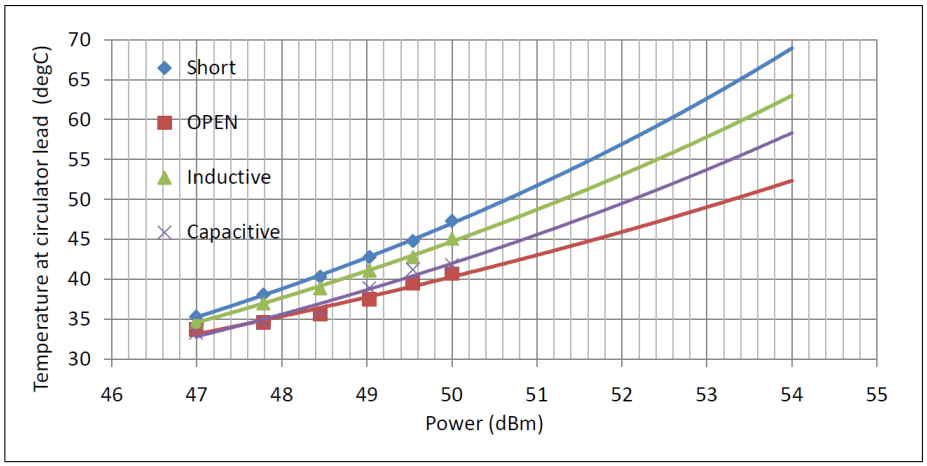

Figure 3.5: Reflections test results

The graph shows the temperature versus power relationship for open, short, inductive, and capacitive test points at the output lead of circulator. The extrapolated trend is rather exponential up to 250 W power. It should be noted that the maximum temperature rise is observed in short circuit condition, where the current phase is maximum and the voltage phase in minimum. Similarly the lowest temperature rise is observed in open circuit condition, where the voltage phase is maximum and the current phase is minimum. The rest of the two graphs lie in between short circuit and open circuit condition. This suggests that the short circuit test condition is sufficient enough for reflections test or ruggedness evaluation. In short circuit condition we have extrapolated temperature of about 70 °C at 250 W (54 dBm) power for 25 °C base temperature of the test fixture.

3.1.5 Outcomes

Experiments with the PCB and the circulator on separate test fixture suggest that they are not the primary cause for this failure. I suspect that the manufacturing or cleaning issues to be the most likely root causes. In faulty PA modules circulator output lead might have not soldered well or might have not cleaned well after the soldering.

Moreover, I recommended improved version of the same PCB called LoPro for 2^{nd} generation PA module design. This PCB has a trace width of about 1.7 mm at our application frequency of 2.5 GHz, which improves the power handling capability of RF traces. Consequently, the burnout issues are solved in 2^{nd} generation PA modules.

3.2 RF power detector

The team has developed a power detector for the SSMO system. The power detector monitors the flow of RF power to and from the PA module and oven cavity. It measures real time forward and reflected RF powers from the PA module and translate them in to respective forward and reflected voltages. Subsequently these measured voltages are digitally processed with the help of small signal board (SSB).

This provides a real time feedback for the SSMO system. The system can decrease the RF power at the input of the PA module in case of high reflected power from the oven cavity. This limits excessive power flow and avoids potential burnouts due to resistive heating of RF traces inside the PA modules. I characterize the output of the power detector for measured forward and reflected voltages with respect to RF power flow to and from the oven cavity.

3.2.1 Design

This power detector is capable of measuring powers up to 1 kW in 2.45 ± 0.05 GHz of frequency range. The detector IC *AD8314* from Analog devices [42] used in the design is essentially a logarithmic amplifier. Figure 3.6 presents the block diagram for the detector. The output voltage of this detector is a log function of the input voltage, and the dynamic range directly comes from the detector itself which is -45 dBm to 0 dBm in 50 Ω environment. There is present an attenuation of 60 dB from the main line of the coupler to the detector in each forward and reverse path, which makes it possible for *AD8314* to measure from 1 kW (60 dBm) to 30 mW (15 dBm).

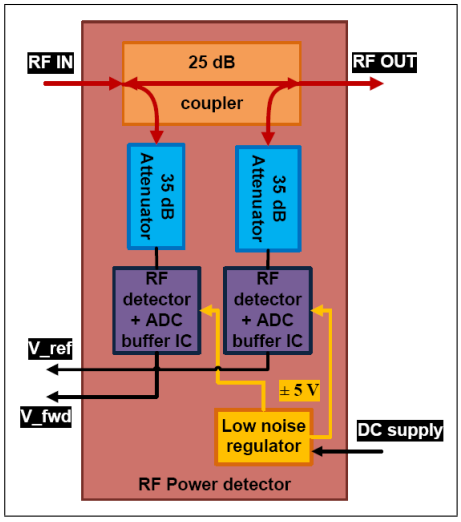

Figure 3.6: Detector block diagram

Analog to digital converter (ADC) *MAX4488* from Maxim [43] is also utilized in the design. The ADC is essentially an operational amplifier operating as non-inverting configuration. It also has a voltage gain of five for scaling up the measured voltages from 1 V to 5 V. This technique is also referred as voltage scaling. The circuit is realized on the PCB *R04350B* from Rogers [41]. The RF detector is enclosed in two separate metal boxes to improve isolation and shielding between analog and digital parts of the circuit. A 25 dB coupler and 35 dB attenuators are enclosed in one metal box namely *coupler block*, and the detector IC and SSB are enclosed in other metal box namely *detector block*. The RF detector operates at $+5$ V_{dc} and measures RF power in terms of forward and reverse voltages.

3.2.2 Characterization

Characterization of the RF power detector is performed in two steps. The first step deals with the measurements of the coupler block separately. The second step deals with the measurements of the detector block connected to the coupler block. The measurement results of the coupler block are presented in Figure 3.7. This coupler is measured using network analyzer for isolation, coupling and directivity. First the network ana-

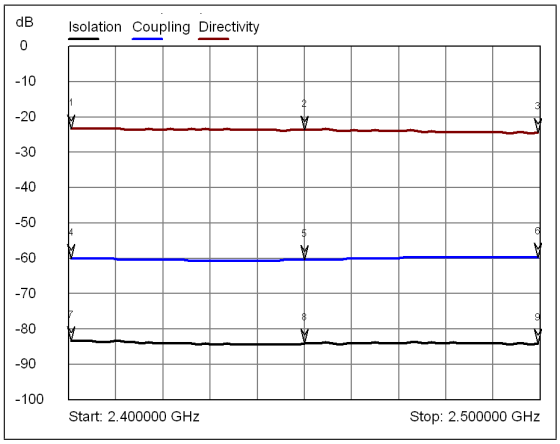

Figure 3.7: Coupler measurements

lyzer is calibrated in frequency range of 2.4 GHz to 2.5 GHz, and then S-parameters are extracted from the coupler block. Table 3.1 summarizes the performance specifications for the coupler.

Table 3.1: Coupler specifications

Parameter	Frequency (MHz)			
(dB)	2400	2450	2500	specs
Coupling	59.9	60.4	59.7	60 dB
Isolation	83.2	84.0	84.0	83 dB
Directivity	23.3	23.6	24.2	23 dB

Next a measurement setup presented in figure 3.8 was built for the characterization of the detector circuit. In this setup power sensors are used for making reference

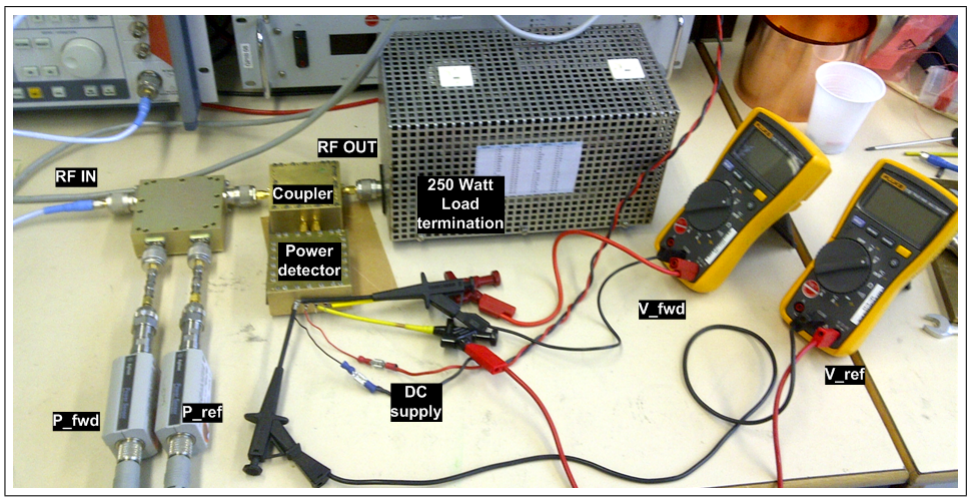

Figure 3.8: Detector measurement setup

measurements for input powers from 1 W to 250 W. The two sets of measurements are performed namely *matched* and *open* conditions. First set of measurements are done by connecting a load at the output of the coupler (matched), and the other set without the load (open). Figure 3.9 presents the measurement results for detector characterization. In this graph the measured forward (V_{fwd}) and reverse (V_{ref}) voltages from the detector are plotted against power readings from the sensors, both for matched and open conditions. The measured voltages show a strong linear behavior with respect to powers in logarithmic scale. A slope of

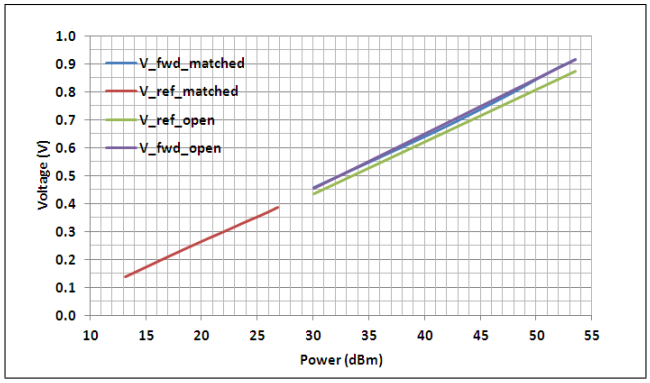

Figure 3.9: Characterized RF power detector

19 mV/dB is being observed, which is in agreement with the datasheet specification of the detector.

3.3 Summary

Analysis of the faulty PA modules is conceivably the least successful task because it did not lead us to a certain conclusion. Although we did manage to produce a detailed Ishikawa diagram corresponding to our particular problem, however at the end we suspected that soldering or cleaning issues could be the most likely root cause of the problem.

On the other hand, a successful attempt was made to realize a working prototype for the RF power detector. Although it took significant amount of time and efforts to get the detector working, nevertheless the measurement results are well up to the specifications. This detector is good enough for the integration inside the 2^{nd} generation PA module design.

4. COMPARISON OF CIRCULATORS FOR 2ND GENERATION PA MODULES

This chapter presents the comparison of five different circulators for 2nd generation PA modules. The comparison is based on formulated test cases specific to our target application. In the application (microwave oven), the PA module will hardly ever see a matched load condition, and most of the time it will deliver power to mismatched loads inside the oven cavity. For this purpose a circulator is used to protect the PA module from the varying load conditions.

There are two key challenges for the PA module design in this application. First one is the high temperature of the environment, the base plate and PCB are expected to have an ambient temperature of 65 °C. Second one is the reflections from the loads. The PA module will face reflections at its output all the time during its operation. Consequently the circulator will handle high forward and reflected powers to and from the oven cavity.

Conventionally the ports of a circulator are characterized for matched load conditions at room temperature. Suppliers do not provide enough information about the behavior of the device during the operation in mismatched loads. Furthermore, we want to make sure that the circulator we use survives the extreme reflections without degrading its performance. Hence we selected five circulators from different suppliers and made a comparison in order to pick the best one for the 2nd generation PA module design.

Section 4.1 presents the formulated test cases for the comparison, namely *ruggedness test* and *S-parameters extraction*. The characterization of a tuner for the ruggedness test is presented in section 4.2. The measurement test bench is presented in section 4.3. Section 4.4 presents the measurement results from each circulator namely *Mesl*, *Partron*, *Trak*, *Renaissance*, and *Dorado* respectively. Comparison of the circulators is presented in section 4.5, and a summary is presented in section 4.6.

Table 4.1 presents the circulators selected for the comparison. Their respective suppliers, part numbers, prices, along with their electrical specifications, and package dimensions are tabulated here. For more information about the circulators see datasheets in Appendix A. The comparison is divided into two parts. One is the

Table 4.1: Circulators selected for the comparison

ITEM	UNITS	1	2	3	4	5
Supplier	-	MESL	Partron	Trak	Renaissance	Dorado
Part#	-	SZM 10497	DCB 2450L4	C2425 LF/J	3G4 NEM	3CD-2.45 -5BW4.1
Unit price	1K pcs	10.80	11.03	13.90	tbd	28.46
(USD)	10K pcs	7.25	08.04	12.10	tbd	19.12
Electrical specifications						
Frequency range	MHz	2400-2500	2400-2500	2400-2500	2400-2500	2400-2500
Insertion loss	dB	0.20	0.30	0.30	0.50	0.30
Isolation	dB	20	20	20	20	20
Return loss	dB	20	20	20	19	20
Power (avg.)	Watt	250	500	250	300	300
Operating temp.	°C	-20,+80	-40,+80	-10,+90	-10,+70	-10,+70
Package dimensions						
Size	LxWxh (mm)	19.05x 19.05x8	19.05x 19.05x8	19.05x 19.05x10	19.05x 19.05x5.6	19.05x 19.05x6.35
Pin type	flat	Angled	Leveled	Angled	Leveled	Leveled
Pin height	mm	2.0	3.0	2.0	3.0	2.5

thermal comparison, and other is the S-parameters comparison. The qualification criteria for the circulators are their electrical and thermal performance, geometry and cost.

4.1 Test cases for the comparison

Figure 4.1 presents the simplified block diagrams for *ruggedness test* and *S-parameter extraction*. The basic principle behind the ruggedness test is similar to the approach presented in section 3.1.4 where the output of a circulator is tested for high reflections. Two test points namely *open circuit (OC)* and *short circuit (SC)* are devised for the test-fixtures. A network analyzer is utilized to characterize a slug tuner for these two test points.

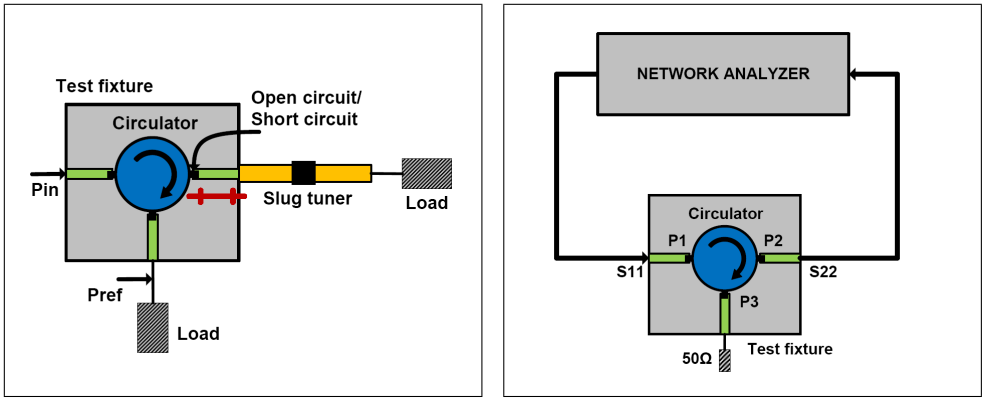

(a) Ruggedness test (b) S-parameter extraction

Figure 4.1: Test cases block diagrams

An input power (P_{in}) sweep is performed from 50 W to 150 W, and temperature is measured at each circulator output. The measurement data is extrapolated up to 250 W using linear curve fitting technique because the slug tuner cannot handle high power. Table 4.2 summarize the formulated test cases for the comparison.

Table 4.2: Test cases for the comparison

(a) RUGGEDNESS TEST		
Circulator Output	-	Open circuit/Short circuit
Frequency	GHz	2.45
RF Power (CW)	Watt	50 - 150 (5 steps)
Time	Sec	60 - 90 / step
Ambient Temperature	°C	25 approx.
(b) S-PARAMETER EXTRACTION		
For examining the behavior of the device before and after the ruggedness test.		

The S-parameter extraction is performed for each test-fixture before and soon after the ruggedness test to observe any degradation in the electrical performance of the circulator. The key parameters involved in S-parameter extraction are insertion loss (S_{21}), isolation (S_{12}), input return loss (S_{11}), and output return loss (S_{22}) from each test-fixture.

4.2 Slug tuner characterization

The most critical aspect of the ruggedness test is to precisely create open circuit (OC) and short circuit (SC) conditions at the output lead of a circulator inside the test-fixture. The *port-extension* option available in the network analyzer [44, p. 217] makes it possible to shift the measurement reference plane inside the test-fixture. This is a two step procedure in which conventional coaxial calibration is performed first. Then reference plane is shifted by entering the desired length and related parameters in the advanced options of the network analyzer.

Next a double slug tuner [45] is utilized to characterize OC and SC points at the output lead of the circulator. A double slug tuner has two degrees of freedom. Both the magnitude and phase of the VSWR can be changed at certain frequency by adjusting the two sliders along the length of the tuner. Figure 4.2 presents the characterized OC and SC points on the Smith chart. It should be noted from the figure that a VSWR ≈ 73 or $|\Gamma| = 0.97$ is achieved for open circuit, and a VSWR ≈ 34 or $|\Gamma| = 0.94$ is achieved for short circuit at 2.45 GHz, respectively. Ideally reflection coefficient (Γ) approaches to unity in both cases which in practice is a remote situation.

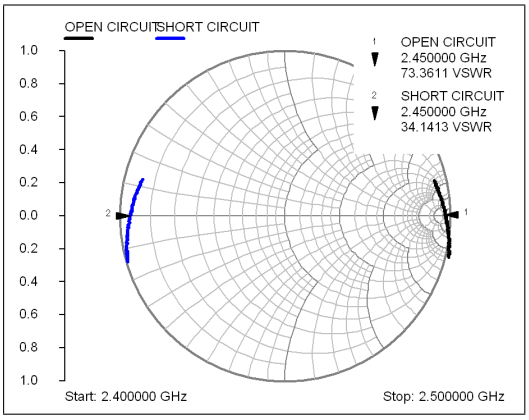

Figure 4.2: Slug tuner characterization

4.3 Measurement test bench

Figure 4.3 presents the test bench prepared for the measurements. The input power is fed from the signal generator following a linear amplifier. The linear amplifier is used because signal generator is not able to deliver enough power for the minimum input drive for the PA module. Directional couplers and power sensors are used for measuring the input power (P_{in}) and the reflected power (P_{ref}) from first and third port of the circulator, respectively.

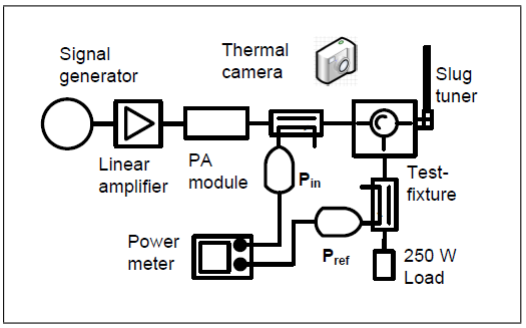

Figure 4.3: Measurement test bench

The test-fixture is placed on a heat sink to keep its temperature roughly at room temperature during the measurements. The characterized slug tuner is connected

at the output of the test-fixture. A thermal camera [46] is placed over the top of the test-fixture to measure temperatures at the output of the circulator. A 250 W load is used for dissipating the reflected power (P_{ref}) from the third port of the circulator.

4.4 Measurements of commercial circulators

Measurements from ruggedness test and S-parameters extraction from each test-fixture are presented separately. A black test paint called *Spirex SP102* is used for making thermal measurements. Spirex has measurement range of up to 350 °C and a constant emissivity of 0.95. It is suitable for making high temperature measurements. The output transmission line of each circulator test-fixture is painted with Spirex. In addition, a small spot on metal base is also painted for making reference measurement as depicted in figure 4.4.

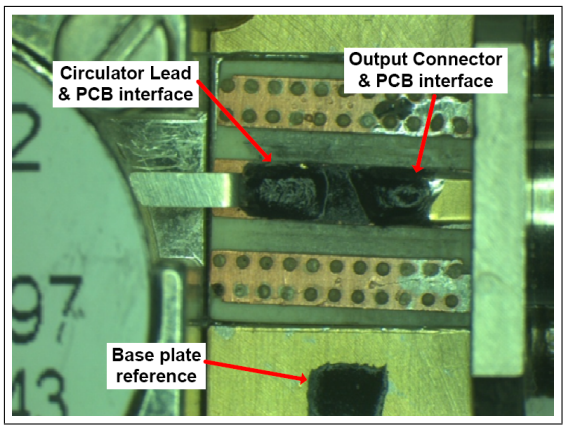

Figure 4.4: Black test paint

I measured temperatures at three points namely *circulator lead*, *output connector*, and *metal base* at every input power level (P_{in}) and in each test case of OC and SC. The results are plotted as temperature rise (ΔT,^{c} o) above the metal base temperature. Consequently the variations of different metal base temperatures are cancelled out among the test-fixtures.

4.4.1 MESL

Figure 4.5 presents the thermal measurements of *Mesl* test-fixture. It should be observed from the graph that at input power $P_{in} = 150$ W, the temperature rise of *circulator lead* is $\Delta T = 76.8$ °C for short circuit (SC) test, and $\Delta T = 50.0$ °C for open circuit (OC) test respectively. Likewise, the temperature rise of *output connector* is $\Delta T = 73.0$ °C for short circuit (SC) test, and $\Delta T = 56.5$ °C for open circuit (OC) test respectively. The reference set of *Mesl* thermal data is available in Appendix B.

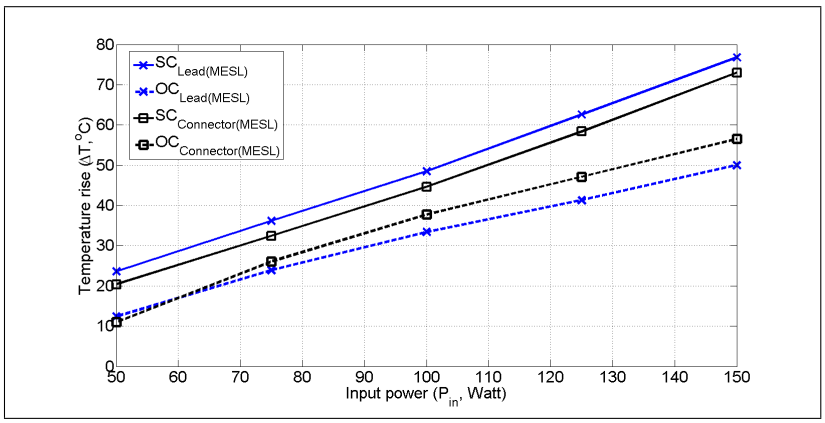

Figure 4.5: MESL thermal measurements

Figure 4.6 presents the S-parameter measurements of MESL test-fixture. It should be noted from the figure 4.6(a) that the input return loss (S_{11}) is above

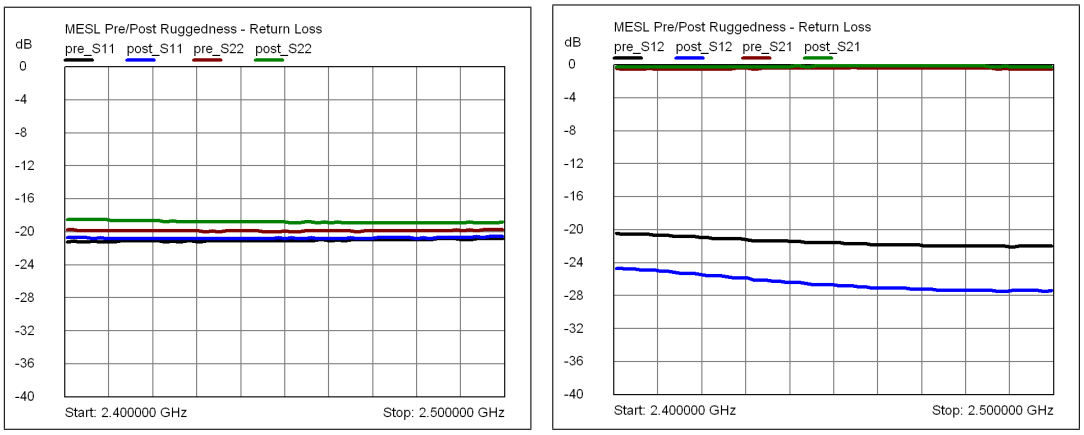

(a) Input and Output return losses (b) Insertion loss and Isolation

Figure 4.6: MESL S-parameter measurements

20 dB before and after the ruggedness test. However, the output return loss (S_{22}) is about 20 dB before the test, and it is about 19 dB after the test respectively. Similarly in figure 4.6(b), the insertion loss (S_{21}) is about 0.3 dB before and after the ruggedness test. However, the isolation (S_{12}) is above 20 dB before the test, and it is above 24 dB after the test respectively.

4.4.2 Partron

Figure 4.7 presents the thermal measurements of *Partron* test-fixture. It should be observed from the graph that at input power $P_{in} = 150$ W, the temperature rise of *circulator lead* is $\Delta T = 76.5$ °C for short circuit (SC) test, and $\Delta T = 45.4$ °C for open circuit (OC) test respectively. However, the temperature rise of *output connector* is $\Delta T = 106.2$ °C for short circuit (SC) test, and $\Delta T = 63.2$ °C for open circuit (OC) test respectively. The poor soldering of the output connector could possibly be the cause of unusual temperature rise in Partron test-fixture. The reference set of *Partron* thermal data is available in Appendix B.

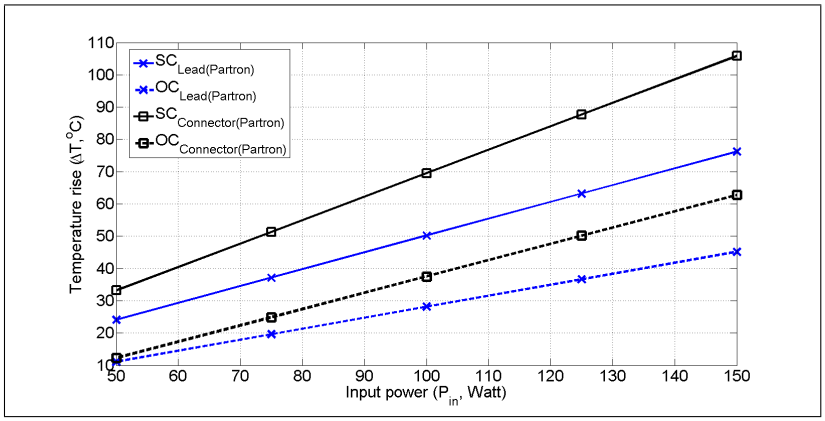

Figure 4.7: Partron thermal measurements

Figure 4.8 presents the S-parameter measurements of Partron test-fixture. It should be noted from the figure 4.8(a) that both the input return loss (S_{11}) and the

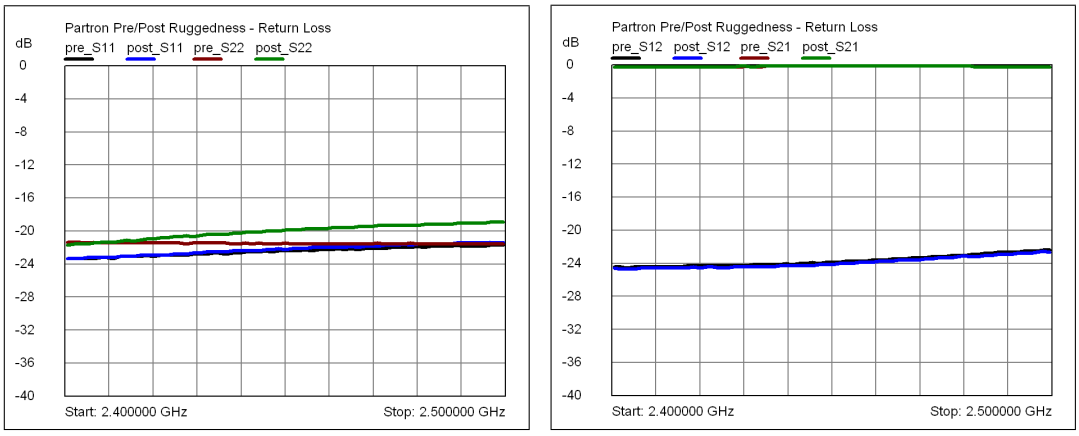

(a) Input and Output return losses (b) Insertion loss and Isolation

Figure 4.8: Partron S-parameter measurements

output return loss (S_{22}) is better than 20 dB before the ruggedness test. However, the output return loss (S_{22}) is about 19 dB after the test. Moreover in figure 4.8(b), the insertion loss (S_{21}) is 0.35 dB and the isolation (S_{12}) is 22 dB respectively, before and after the ruggedness test.

4.4.3 TRAK

Figure 4.9 presents the thermal measurements of *Trak* test-fixture. It should be observed from the graph that at input power $P_{in} = 150$ W, the temperature rise of *circulator lead* is $\Delta T = 71.8$ °C for short circuit (SC) test, and $\Delta T = 53.5$ °C for open circuit (OC) test respectively. Likewise, the temperature rise of *output connector* is $\Delta T = 67.5$ °C for short circuit (SC) test, and $\Delta T = 53.1$ °C for open circuit (OC) test respectively. The reference set of *Trak* thermal data is available in Appendix B.

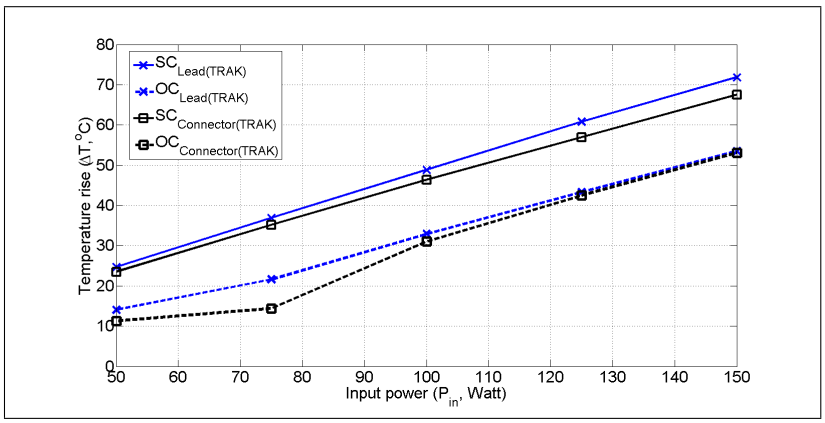

Figure 4.9: TRAK thermal measurements

Figure 4.10 presents the S-parameter measurements of TRAK test-fixture. It should be noted from the figure 4.10(a) that both the input return loss (S_{11}) and

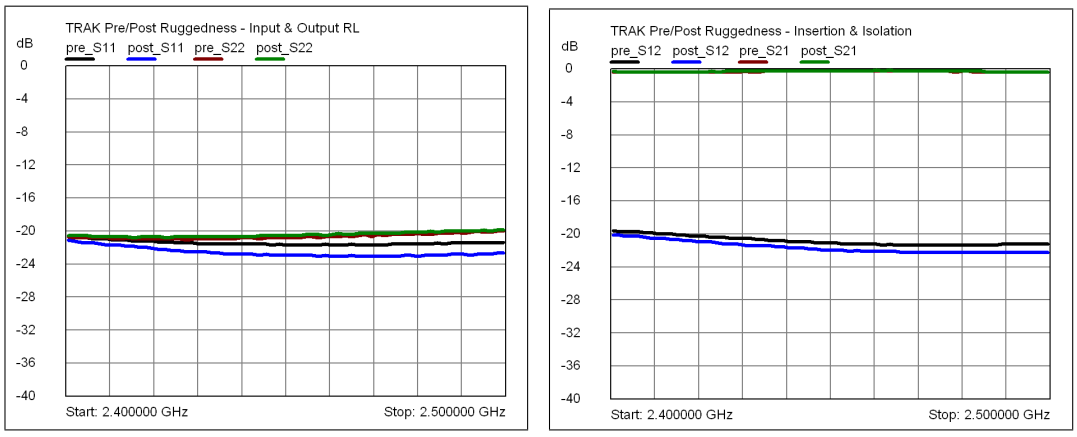

(a) Input and Output return losses (b) Insertion loss and Isolation

Figure 4.10: TRAK S-parameter measurements

the output return loss (S_{22}) is about 20 dB before and after the ruggedness test. Similarly in figure 4.10(b), the insertion loss (S_{21}) is 0.5 dB and the isolation (S_{12}) is about 20 dB, before and after the ruggedness test.

4.4.4 Renaissance

Figure 4.11 presents the thermal measurements of *Renaissance* test-fixture. It should be observed from the graph that at input power $P_{in} = 150$ W, the temperature rise of *circulator lead* is $\Delta T = 73.5$ °C for short circuit (SC) test, and $\Delta T = 62.0$ °C for open circuit (OC) test respectively. Likewise, the temperature rise of *output connector* is $\Delta T = 63.6$ °C for short circuit (SC) test, and $\Delta T = 66.0$ °C for open circuit (OC) test respectively. The reference set of *Renaissance* thermal data is available in Appendix B.

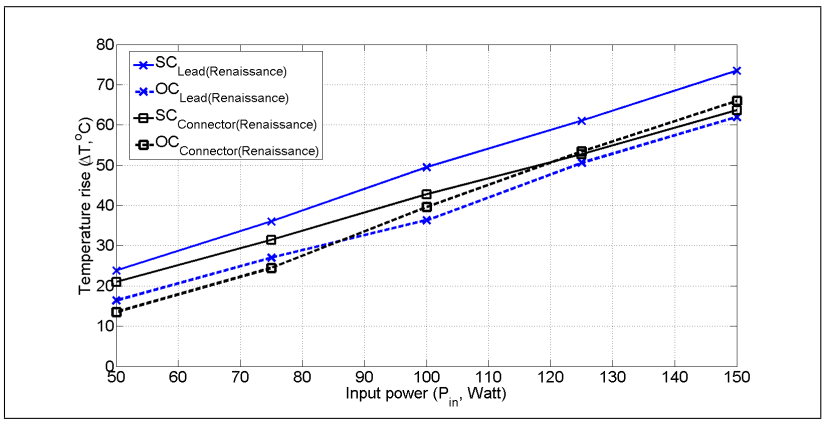

Figure 4.11: Renaissance thermal measurements

Figure 4.12 presents the S-parameter measurements of Renaissance test-fixture. It should be noted from the figure 4.12(a) that both the input return loss (S_{11}) and

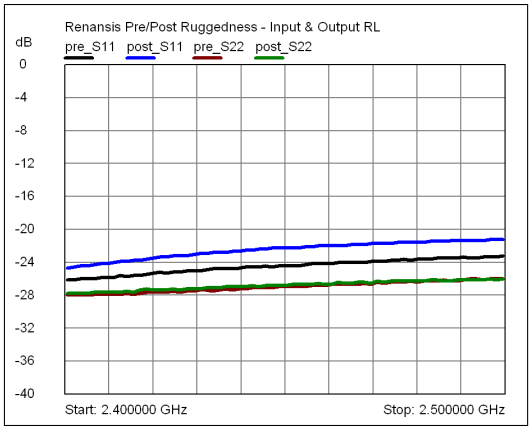

(a) Input and Output return losses

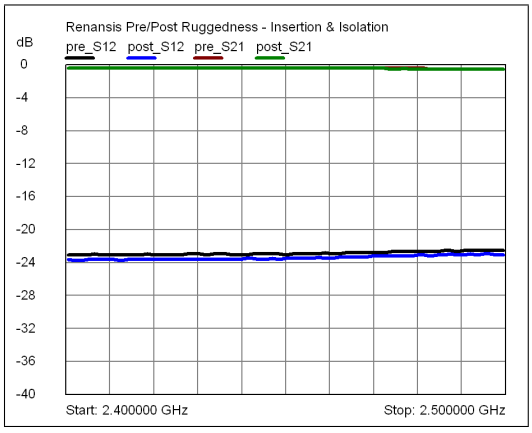

(b) Insertion loss and Isolation

Figure 4.12: Renaissance S-parameter measurements

the output return loss (S_{22}) is better than 21 dB before and after the ruggedness test. Similarly in figure 4.12(b), the insertion loss (S_{21}) is 0.6 dB and the isolation (S_{12}) is about 23 dB, before and after the ruggedness test.

4.4.5 Dorado

Figure 4.13 presents the thermal measurements of *Dorado* test-fixture. It should be observed from the graph that at input power $P_{in} = 150$ W, the temperature rise of *circulator lead* is $\Delta T = 65.2$ °C for short circuit (SC) test, and $\Delta T = 44.4$ °C for open circuit (OC) test respectively. Likewise, the temperature rise of *output connector* is $\Delta T = 80.4$ °C for short circuit (SC) test, and $\Delta T = 57.6$ °C for open circuit (OC) test respectively. The reference set of *Dorado* thermal data is available in Appendix B.

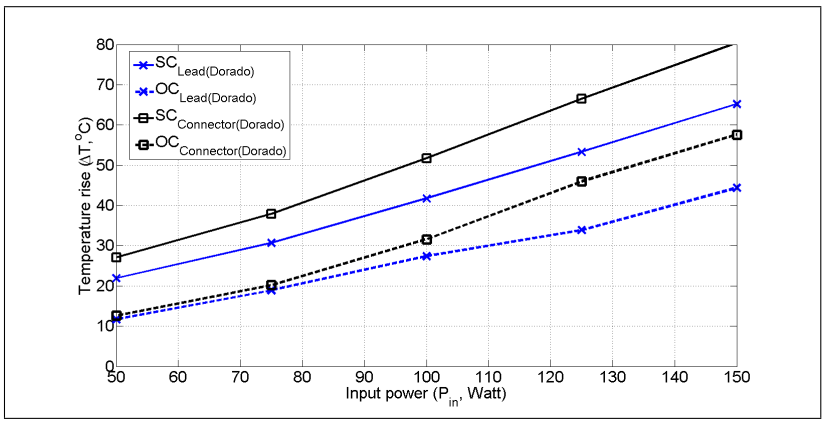

Figure 4.13: Dorado thermal measurements

Figure 4.14 presents the S-parameter measurements of Dorado test-fixture. It

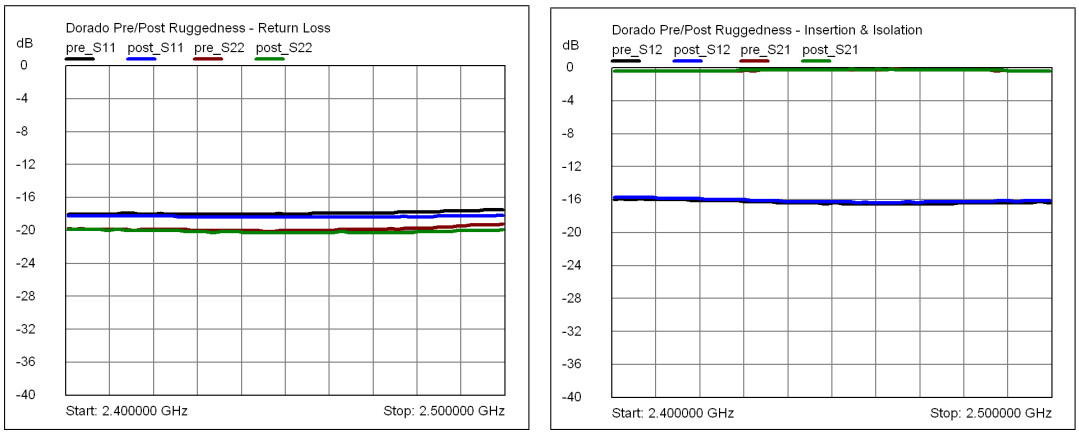

(a) Input and Output return losses (b) Insertion loss and Isolation

Figure 4.14: Dorado S-parameter measurements

should be noted from the figure 4.14(a) that both the input return loss (S_{11}) and the output return loss (S_{22}) is better than 18 dB before and after the ruggedness test. Similarly in figure 4.14(b), the insertion loss (S_{21}) is 0.4 dB and the isolation (S_{12}) is about 16 dB, before and after the ruggedness test. However this test-fixture is not meeting the datasheet specifications available in Appendix A.

4.5 Comparison of circulators

The thermal performance comparison of the five circulators is presented in figure 4.15. The temperatures are recorded at three points namely *circulator lead, output connector*, and *metal base*. The graphs are plotted as temperature rise (ΔT) above the *metal base* temperature at *circulator lead* in figure 4.15(a), and at *output connector* in figure 4.15(b). The input power (P_{in}) used during the measurements is from 50 W to 150 W and further extrapolated up to 250 W using linear curve

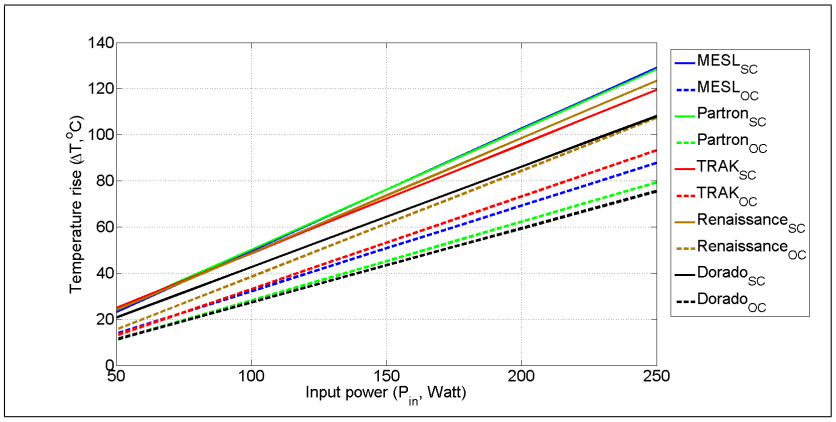

(a) Circulator lead and PCB interface

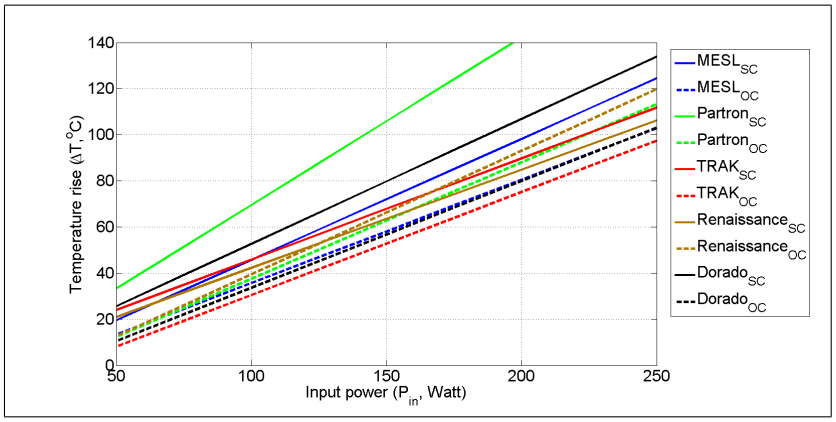

(b) Output connector and PCB interface

Figure 4.15: Thermal comparison of circulators

fitting. This can be justified using the equation (2.23) which also implies that the temperature rise is directly proportional to the incident power in a microstrip conductor, if all the other physical conditions remain unchanged. It should be noted from the figures that the short circuit (SC) test results are presented as solid line graphs, and the open circuit (OC) test results are presented as dotted line graphs for each circulator. Moreover, the color code is blue for MESL, green for Partron, red for TRAK, brown for Renaissance, and black for Dorado respectively.

It should also be noted from the figure 4.15(a) that the temperature rise (ΔT) for SC tests are higher than OC tests at *circulator lead* in every test-fixture measure-

ments. Consequently the circulator test-fixture with least temperature rise (ΔT) in short circuit test is considered to exhibit a superior thermal performance over its counter-parts.

As discussed earlier in section 4.4.5 that the Dorado test-fixture is not meeting the datasheet specifications. Possible explanation could be that we have received a poor sample from Dorado. We carried out the measurements with this sample because another sample from Dorado was not available at that time. Consequently we grade the thermal and electrical measurement results from Dorado test-fixture as defective. However based on the experiments with other test-fixtures we believe that a good sample from Dorado would also exhibit a thermal and an electrical performance close to its counter-parts.

Table 4.3 presents the extrapolated ΔT at *circulator lead* and *output connector* for 250 W input power. It is clear from the comparison results that the TRAK circulator exhibit the best thermal performance (extrapolated $\Delta T = 119$ °C) in SC test. There is about 10 °C of difference between the extrapolated ΔT of TRAK at circulator lead from that of MESL and Parton circulator leads in the SC test.

Table 4.3: Thermal comparison of circulators

ITEM	UNITS	MESL	Partron	Trak	Renaissance	Dorado
Ruggedness test (Pin = 250 W, extrapolated ΔT at circulator lead)						
Short circuit	°C	129	128	119	123	108
Open circuit	°C	88	79	93	107	76
Ruggedness test (Pin = 250 W, extrapolated ΔT at output connector)						
Short circuit	°C	124	>140	112	106	134
Open circuit	°C	103	113	97	120	103

On the other hand, the ΔT at *output connector* is rather arbitrary in SC and OC measurements. Particularly in case of Partron test-fixture the extrapolated ΔT in SC test is much higher than 140 °C. Moreover in case of Renaissance test-fixture the extrapolated ΔT is 106 °C in SC test, which is even lower than the extrapolated ΔT of 120 °C in OC test. We have observed that the soldering of the output connector plays a critical role in defining the output return loss (S_{22}) of the test-fixture, and has a significant effect on thermal measurements at *output connector*. A poorly soldered connector at the output of the test-fixture degrades the output return loss (S_{22}) and increases the temperature rise (ΔT).

The electrical performance comparison of the five circulators is presented in figure 4.16. The S-parameters are extracted from each test-fixture after the ruggedness tests and the thermal measurements. Figure 4.16(a) presents the insertion loss (S_{21}), figure 4.16(b) presents the isolation (S_{12}), figure 4.16(c) presents the input return loss (S_{11}), and figure 4.16(d) presents the output return loss (S_{22}) respectively.

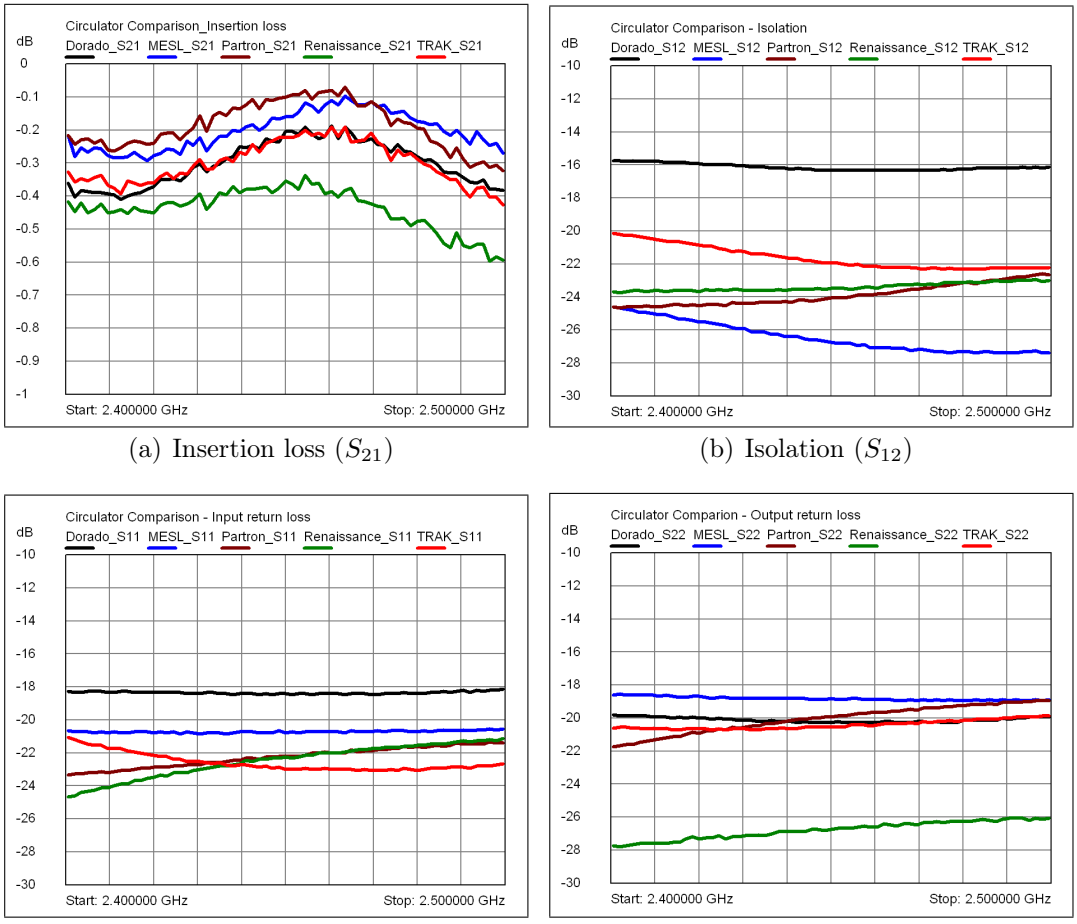

(a) Insertion loss (S_{21})

(b) Isolation (S_{12})

(c) Input return loss (S_{11})

(d) Output return loss (S_{22})

Figure 4.16: S-parameter comparison of circulators

The least value is considered from each parameter as its minimum performance within the frequency range from 2.40 GHz to 2.50 GHz. It should be noted that four of the five circulator test-fixture measurements are in agreement with their respective datasheet specifications. However Dorado test-fixture is out of specification in isolation and return loss.

Table 4.4 presents the measured S-parameters from each circulator test-fixture along with their datasheet specifications.It should be noted that the MESL test-

Table 4.4: S-parameter comparison of circulators

ITEM	UNITS	MESL	Partron	Trak	Renaissance	Dorado
Electrical specifications from suppliers						
Insertion loss	dB	0.2	0.3	0.3	0.5	0.3
Return loss	dB	20	20	20	19	20
Isolation	dB	20	20	20	20	20
S-parameters after ruggedness test (Frequency = 2400 - 2500 MHz)						
Insertion loss	dB	0.3	0.3	0.4	0.6	0.4
Return loss	dB	19	19	20	21	18
Isolation	dB	24	23	20	23	16

fixture exhibits best isolation of 24 dB among others. Similarly the Renaissance test-fixture exhibits the best return loss of 21 dB. However the insertion losses are almost same for each circulator test-fixture.

4.6 Summary

A successful comparison is made for thermal performance and electrical performance of five circulators from different suppliers in the application specific test cases. The qualification criteria of a circulator for 2^{nd} generation PA module design is its electrical and thermal performance. Moreover, circulators from different suppliers are also competing with one another in terms of their geometry and unit price. This means that a trade-off can be made between performance and cost.

Based on the measurements results of circulator test-fixtures and their comparison, *Trak circulator* test-fixture exhibits the best thermal performance. Unfortunately *Dorado circulator* test-fixture is disqualified due to the poor sample delivery from the supplier. On the other hand, *Mesl circulator* test-fixture exhibits the best electrical performance in terms of isolation, and it has the lowest cost per unit price. Consequently, we have selected *Mesl circulator* for 2^{nd} generation PA module design.

5. CONCLUSION

The SSMO project exploits solid-state technology for heating applications. Such a cooking device will be an intelligent system that can change output power, frequency, and signal phase. Consequently, this device will provide better cooking experience to the customers. To this date the project is still in its early phases, and developments are on their way.

I contributed in the developments of the power amplifier module designed for the SSMO system. My key accomplishments are the analysis of faulty PA modules, characterization of RF power detector, and comparison of circulators. The analysis of faulty PA modules was perhaps the least successful task. Rigorous treatment of the analysis and some experimentation did not lead us to the exact root cause of the failure. However, a successful attempt is made to realize a working prototype of the RF power detector. The presented measurement results for power detector characterization are up to the expectations.

The comparison of circulators is based on their thermal and electrical performance in application specific test cases. Various preparations and procedures were carried out to successfully conduct the comparison. The preparation of identical test-fixtures and ordering the samples from the suppliers consume significant amount of time. Another challenging task was to characterize the tuner for open circuit and short circuit test condition. Furthermore preparing the circulator test-fixtures for thermal measurements took days before the actual measurements started. Even so the final results that are reported here have their limitations. For instance the results from Dorado test-fixture are discredited because of the poor circulator unit. Moreover the measurement data is extrapolated to observe the trend rather than taking the actual measurements up to 250 W input power.

The main future task is to redesign the PA module. Integration of the power detector inside the PA module is necessary to monitor the RF power flow to and from the oven cavity. This will provide a lasting solution to burnouts observed in the current PA modules. Another future task is to order a good quality sample from Dorado and perform the circulators comparison again. Furthermore, measure the thermal performance of each circulator test-fixture up to 250 W input power rather than extrapolating the measurement data. It would be interesting to observe the validity of the results presented here.

On the completion of this thesis work, I gained in-depth understanding of SSMO systems. I was exposed to the design of PA module in particular, and SSMO system in general. I also got hands on experience with the instruments which I never used before, such as infra-red camera for thermal imaging. In the theory part, I have gained fine understanding of power amplifier basics, theory of circulators and directional couplers. I understood the key performance parameters related to these devices, and learned techniques to measure those parameters in the lab.

BIBLIOGRAPHY

[1] F. Leens, "An introduction to I2C and SPI protocols," *Instrumentation Measurement Magazine, IEEE*, vol. 12, no. 1, pp. 8 –13, february 2009.

[2] "White paper: Introduction to JTAG Boundary Scan, Corelis." http://www.corelis.com/whitepapers/Boundary-Scan_Whitepaper.pdf, cited on 24.10.2012.

[3] "Application note: Boundary-Scan for PCB Interconnect Testing, Sun Microelectronics." http://canarie.co.in/boundaryscantester.pdf, cited on 24.10.2012.

[4] "Datasheet: BLF25M612G Power LDMOS transistor, NXP Semiconductors." http://www.nxp.com/documents/data_sheet/BLF25M612G.pdf, cited on 24.10.2012.

[5] "Datasheet: BLF2425M7LS250P Power LDMOS transistor, NXP Semiconductors." http://www.nxp.com/documents/data_sheet/BLF2425M7L250P_2425M7LS250P.pdf, cited on 24.10.2012.

[6] K. Ishikawa, *Guide to quality control*, ser. Industrial engineering and technology. Asian Productivity Organization, 1986.

[7] F. Sechi and M. Bujatti, *Solid-State Microwave High-Power Amplifiers*. Artech House, 2009, (ISBN: 978-1-59693-319-4).

[8] P. Colantonio, F. Giannini, and E. Limiti, *High Efficiency RF and Microwave Solid State Power amplifiers*. John Wiley, 2009, (ISBN:978-0-470-51300-2).

[9] M. K. Kazimierczuk, *RF Power Amplifiers*. John Wiley, 2008, (ISBN: 978-0-470-77946-0).

[10] M. Albulet, *RF Power Amplifiers*. Noble, 2001, (ISBN: 1-884932-12-6).

[11] P. B. Kenington, *High-Linearity RF Amplifier Design*. Artech House, 2000, (ISBN:1-58053-143-1).

[12] S. M. Sze, *Semiconductor Devices Physics and Technology*. John Wiley, 2001.

[13] M. Golio, *RF and Microwave Semiconductor Device Handbook*. Boca Raton, 2003.

[14] J. Rogers and C. Plett, *Radio Frequency Integrated Circuit Design*. Artech House, 2003, (ISBN: 1-58053-502-x).

[15] R. G. Carter, *Electromagnetic waves: Microwave components and devices*. Chapman and Hall, 1990, (ISBN: 978-0-442-31183-4).

[16] S. Y. Liao, *Microwave Devices and Circuits*. Prentice Hall, 1985, (ISBN: 978-0-135-81695-0).

[17] J. Helszajn, *The Stripline Circulators: Theory and Practice*. John Wiley, 2008, (ISBN: 978-0-470-26420-1).

[18] R. Weber, *Introduction to Microwave Circuits: Radio Frequency and Design Applications*. John Wiley, 2001, (ISBN: 978-0-470-54500-3).

[19] R. Collin, *Foundations for Microwave Engineering*. John Wiley, 2001, (ISBN: 978-0-470-54466-2).

[20] "Application note: Ferrite isolators and circulators, DITOM Microwave Inc." http://www.ditom.com/Application_Notes.pdf, cited on 24.10.2012.

[21] "Application note: An elementry introduction to ferrite isolators, circulators and rf loads, TX RX Systems Inc." http://www.repeater-builder.com/tx-rx/tx-rx-elementary-introduction-to-ferrite-isolators-circulators-and-rf-loads.pdf, cited on 24.10.2012.

[22] E. Schloemann, "Circulators for microwave and millimeter-wave integrated circuits," *Proceedings of the IEEE*, vol. 76, no. 2, pp. 188 –200, feb 1988.

[23] E. Skomal, "Theory of operation of a 3-port y-junction ferrite circulator," *Microwave Theory and Techniques, IEEE Transactions on*, vol. 11, no. 2, pp. 117 – 122, mar 1963.

[24] C. Fay and R. Comstock, "Operation of the ferrite junction circulator," *Microwave Theory and Techniques, IEEE Transactions on*, vol. 13, no. 1, pp. 15 – 27, jan 1965.

[25] D. M. Pozar, *Microwave Engineering*. John Wiley, 1998, (ISBN: 0-471-17096-8).

[26] S. W. Tee, "Miniature circulators for microwave Integrated circuits," Bachelor thesis, National University of Singapore, 2012. [Online]. Available: http://www.physics.nus.edu.sg/student/Honours%20Projects%20Repository/Soh%20Wee%20Tee.pdf

[27] "Application note: Isolator and circulator basics, MECA Electronics Inc." http://www.e-meca.com/app_notes/Isolator_&_Circulator_Basics.pdf, cited on 24.10.2012.

[28] "Application note: Directional Couplers, Mini Circuits." http://217.34.103.131/app/COUP7-2.pdf, cited on 24.10.2012.

[29] "Application note: Directional Couplers and Bridges, Agilent Technologies." http://www.home.agilent.com/upload/cmc_upload/All/Direct_CouplerOverview.pdf?&cc=FI&lc=fin, cited on 24.10.2012.

[30] "Application note: Understanding directivity, Antrisu Corporation." http://www.electron.frba.utn.edu.ar/~jcecconi/Bibliografia/03%20-%20Medicion%20de%20Potencia%20en%20RF%20y%20micro-ondas/Anritsu_Understanding_Directivity.pdf, cited on 24.10.2012.

[31] "Application note: Straight talk about directivity, Bird Electronic Corporation." http://www.aspen-electronics.com/files/technical/Straight-Talk-About-Directivity.pdf, cited on 24.10.2012.

[32] "Application note: Directivity and VSWR measurements, Marki Microwave." http://www.admiral-microwaves.co.uk/pdf/marki-microwave/directivity_and_vswr_measurements.pdf, cited on 24.10.2012.

[33] "Datasheet: E4416A/E4417A EPM-P Series Power Meters and E-Series E9320 Peak and Average Power Sensors, Agilent Technologies." http://cp.literature.agilent.com/litweb/pdf/5980-1469E.pdf, cited on 24.10.2012.

[34] "Technical tool: Bird RF Calculator , Bird Technologies." http://www.bird-electronic.com/Resources/TechnicalTools.aspx#.UI8f2W-ORvU, cited on 24.10.2012.

[35] I. Bahl and D. K. Trivedi, "A designer's guide to microstrip line," *Microwaves*, pp. 174 – 182, May 1977.

[36] I. Bahl and R. Garg, "Simple and accurate formulas for a microstrip with finite strip thickness," *Proceedings of the IEEE*, vol. 65, no. 11, pp. 1611 – 1612, nov. 1977.

[37] I. Bahl and S. Stuchly, "Analysis of a microstrip covered with a lossy dielectric," *Microwave Theory and Techniques, IEEE Transactions on*, vol. 28, no. 2, pp. 104 – 109, feb 1980.

[38] I. Bahl and K. Gupta, "Average power-handling capability of microstrip lines," *Microwaves, Optics and Acoustics, IEE Journal on*, vol. 3, no. 1, pp. 1 –4, january 1979.

[39] "Application note: Temperature rise estimation in Rogers high frequency circuit boards carrying direct or RF current, Rogers Corporation." http://www.rogerscorp.com/documents/1526/acm/Temperature-Rise-Estimations-in-Rogers-High-Frequency-Circuit-Boards-Carrying-Direc pdf, cited on 24.10.2012.

[40] "Ishikawa diagram — Wikipedia, The Free Encyclopedia," http://en.wikipedia.org/w/index.php?title=Ishikawa_diagram&oldid=536729085, cited on 24.10.2012.

[41] "Datasheet: R04000 LoPro Series, High Frequency Circuit Materials, Rogers Corporation." http://www.rogerscorp.com/documents/1183/acm/RO4000-LoPro-Laminates.pdf, cited on 24.10.2012.

[42] "Datasheet: AD8314 RF Detector, Analog Devices." http://www.analog.com/static/imported-files/data_sheets/AD8314.pdf, cited on 24.10.2012.

[43] "Datasheet: MAX4488 Operational Amplifier, Maxim Integrated." http://datasheets.maximintegrated.com/en/ds/MAX4475-MAX4489.pdf, cited on 24.10.2012.

[44] "User manual: 8719D, 8720D and 8722D Network Analyzer User's Guide,Agilent Technologies." http://cp.literature.agilent.com/litweb/pdf/08720-90288.pdf, cited on 24.10.2012.

[45] "Datasheet: SF-31N Double slug tuner, Microlab." http://fxr.com/applications/~/media/Microlab/Datasheets/SFseries.ashx, cited on 24.10.2012.

[46] "Datasheet: T335 FLIR Infrared Camera, FLIR T-Series." http://www.pat-services.co.uk/downloads/datasheets/1485_Flir_T335_Datasheet.pdf, cited on 24.10.2012.

A. APPENDIX - CIRCULATORS DATASHEETS

Partron

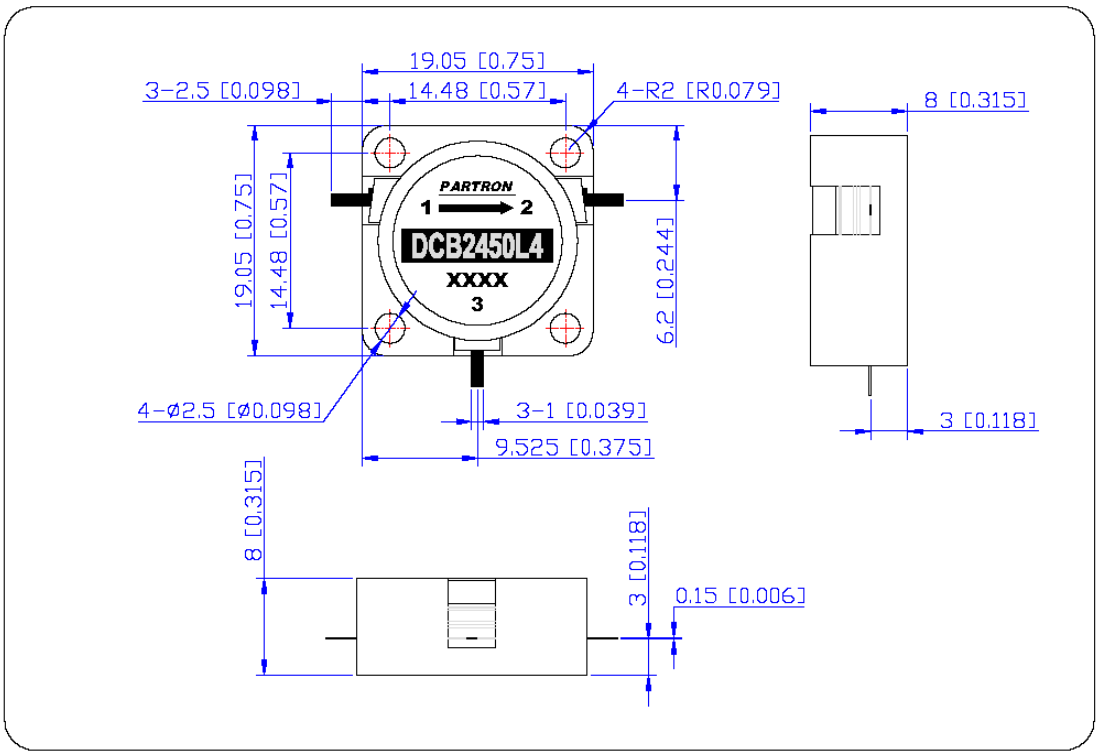

ELECTRICAL SPECIFICATION	
Frequency Range	2400 ~ 2500 MHz
Operating Temp.	-40 ~ +85℃
Insertion Loss	0.25 dB max. (+25 ± 5 ℃) 0.30 dB max. (-40 ~ +85 ℃)
Isolation	23 dB min. (+25 ± 5 ℃) 20 dB min. (-40 ~ +85 ℃)
Return Loss	23 dB min. (+25 ± 5 ℃) 20 dB min. (-40 ~ +85 ℃)
Rating Power	500 W max. (CW)
Impedance	50 Ω

MATERIAL SPECIFICATION
MATERIAL
BODY/LID : STEEL TAB : PHOSPHOR BRONZE
FINISH
BODY/LID : Ni(NICKEL) PLATE TAB : Ag(SILVER) PLATE
- ROTATION : L TYPE(CW) * GENERAL TOLERANCE : ± 0.3mm * DRAWING UNIT : mm[INCH] * RoHS COMPLIANT

partron

represented by:
MRC COMPONENTS

Hoogedijk 10, 1145 PM Katwoude, Nederland
Tel: +31-299-687415
Email: vincent.heuvelsland@mrccomponents.com

MESL

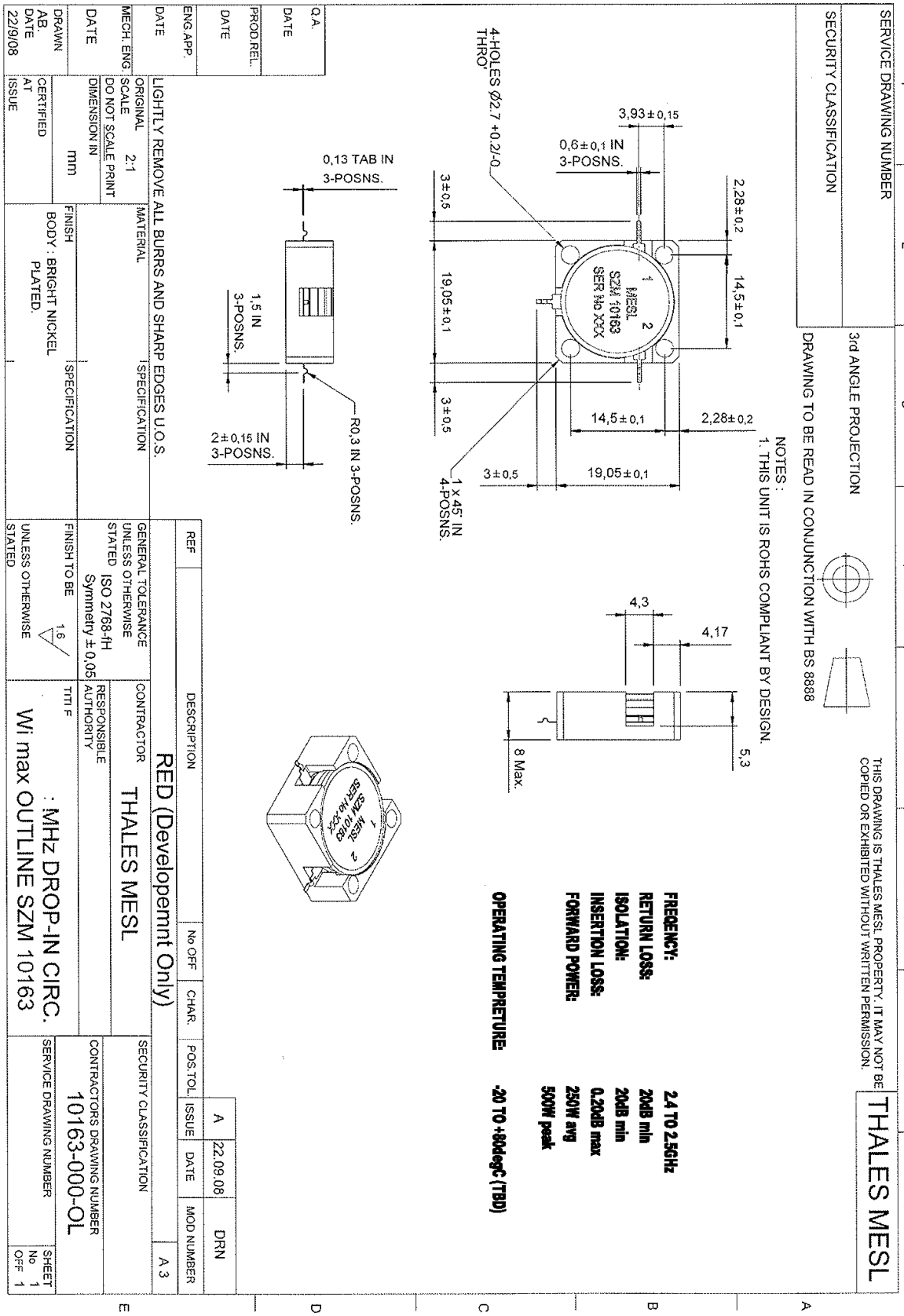
THALES MESL
THIS DRAWING IS THALES MESL PROPERTY. IT MAY NOT BE COPIED OR EXHIBITED WITHOUT WRITTEN PERMISSION.
SERVICE DRAWING NUMBER
SECURITY CLASSIFICATION
3rd ANGLE PROJECTION
DRAWING TO BE READ IN CONJUNCTION WITH BS 8888
NOTES :
1. THIS UNIT IS ROHS COMPLIANT BY DESIGN.
FREQENCY: 2.4 TO 2.5GHz
RETURN LOSS: 20dB min
ISOLATION: 20dB min
INSERTION LOSS: 0.20dB max
FORWARD POWER: 250W avg
500W peak
OPERATING TEMPRETURE: -20 TO +80degC (TBD)
4-HOLES Ø2.7 +0.2/-0 THRO'
3,93 ± 0,15
0,6 ± 0,1 IN 3-POSNS.
2,28 ± 0,2
14,5 ± 0,1
19,05 ± 0,1
3 ± 0,5
1 x 45° IN 4-POSNS.
4,3
4,17
5,3
8 Max.
0,13 TAB IN 3-POSNS.
1,5 IN 3-POSNS.
2 ± 0,15 IN 3-POSNS.
R0,3 IN 3-POSNS.
MESL
SZM 10163
SER No XXX
Q.A.
DATE
PROD.REL.
DATE
ENG.APP.
DATE
MECH. ENG.
DATE
DRAWN
AB.
DATE
22/9/08
ORIGINAL SCALE 2:1
DO NOT SCALE PRINT
DIMENSION IN mm
CERTIFIED AT ISSUE
LIGHTLY REMOVE ALL BURRS AND SHARP EDGES U.O.S.
MATERIAL
SPECIFICATION
FINISH
SPECIFICATION
BODY : BRIGHT NICKEL PLATED.
GENERAL TOLERANCE UNLESS OTHERWISE STATED ISO 2768-fH
Symmetry ± 0,05
FINISH TO BE 1.6
UNLESS OTHERWISE STATED
CONTRACTOR THALES MESL
RESPONSIBLE AUTHORITY
TITLE
: MHz DROP-IN CIRC.
Wi max OUTLINE SZM 10163
REF
DESCRIPTION
No OFF
CHAR.
POS.TOL
ISSUE
DATE
MOD NUMBER
DRN
A
22.09.08
RED (Developemnt Only)
SECURITY CLASSIFICATION
A 3
CONTRACTORS DRAWING NUMBER
10163-000-OL
SERVICE DRAWING NUMBER
SHEET No 1 OFF 1

Renaissance

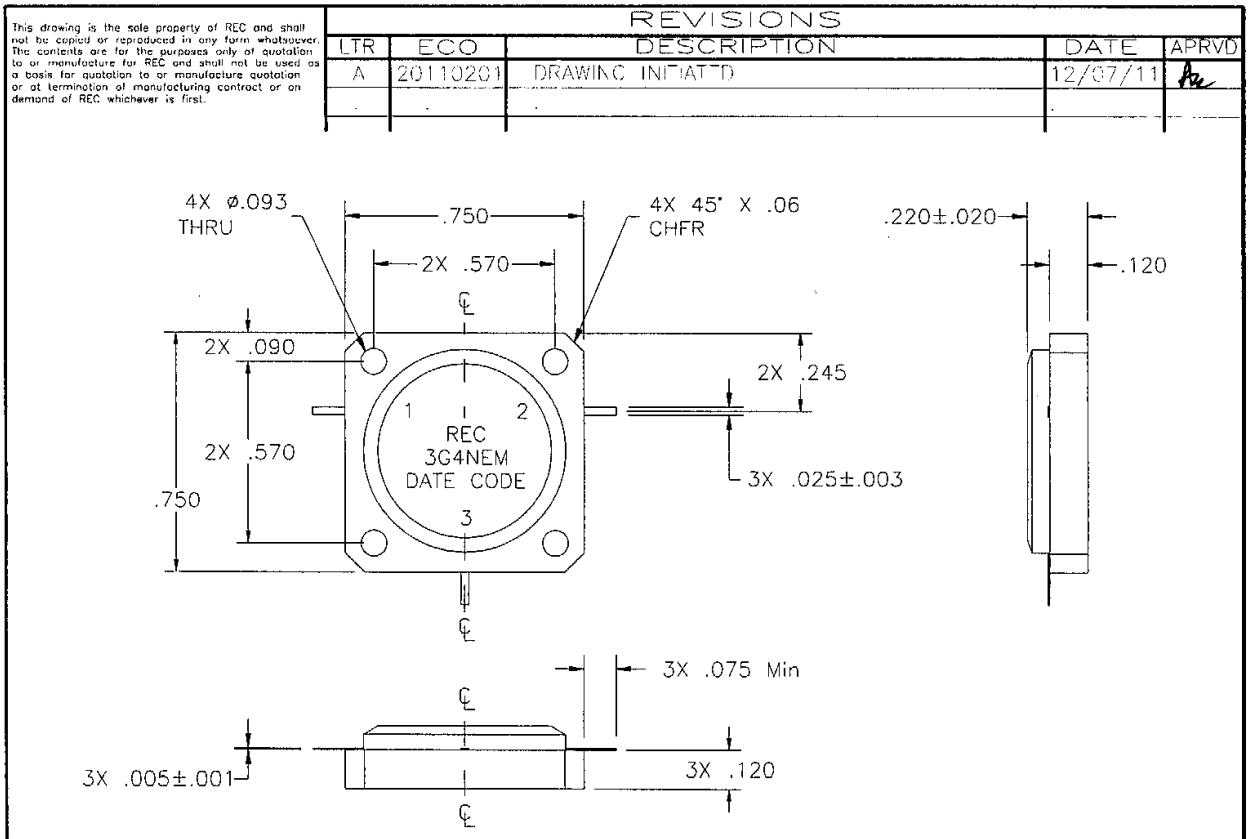

ELECTRICAL CHARACTERISTICS:

FREQUENCY RANGE	2.4 – 2.5 GHz
ISOLATION (Min)	20 dB
INSERTION LOSS (Max)	0.5 dB
VSWR (Max)	1.25 : 1
POWER	300 Watts (AVG)
TEMPERATURE RANGE	−10°C TO +70°C

USED ON	UNLESS OTHERWISE SPECIFIED DIMENSIONS ARE IN INCHES	DRAWN	M.MCMILLER DATE 12/07/11	RENAISSANCE ELECTRONICS CORPORATION	12 LANCASTER COUNTY ROAD HARVARD, MA 01451 PHONE: (978)772-7774 FAX: (978)772-7775
	TOLERANCES ON DECIMALS: .X± .02, .XX± .01, .XXX± .005; ANGLES: ±1/2°	CHECKED			
		ENG. APVD	A.SRIVASTAVA 12/07/11	TITLE: CIRCULATOR, DROP-IN	
		MFG. APVD			
CUSTOMER SPECIFICATION # .	UNLESS OTHERWISE SPECIFIED 63 ALL OVER	APPROVALS		SIZE A; CAGE IDENT NO. 0RJ02; DRAWING NO. 3G4NEM	
FILE NAME OD\3G4NEM	NOTE: THIS DWG INCORPORATES THIRD ANGLE PROJECTION			SCALE 2 : 1; DISK #1-44; SHEET 1 OF 1	

TRAK

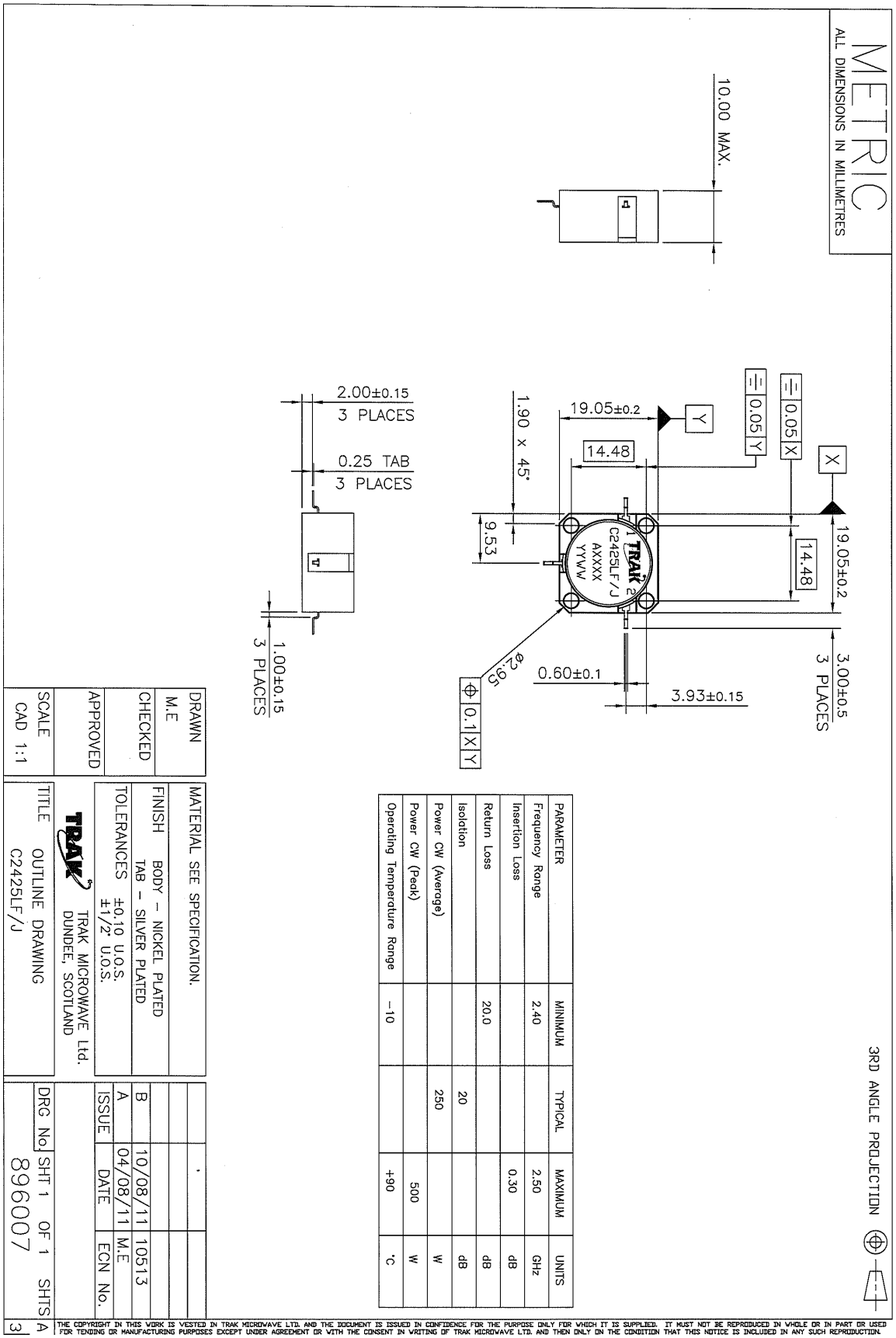
METRIC
ALL DIMENSIONS IN MILLIMETRES
3RD ANGLE PROJECTION
10.00 MAX.
2.00±0.15
3 PLACES
0.25 TAB
3 PLACES
1.90 x 45°
19.05±0.2
14.48
9.53
0.05 X
0.05 Y
X
Y
19.05±0.2
14.48
3.00±0.5
3 PLACES
ø2.95
0.1 X Y
0.60±0.1
3.93±0.15
1.00±0.15
3 PLACES
TRAK
C2425LF/J
AXXXX
YYWW
PARAMETER | MINIMUM | TYPICAL | MAXIMUM | UNITS
Frequency Range | 2.40 | | 2.50 | GHz
Insertion Loss | | | 0.30 | dB
Return Loss | 20.0 | | | dB
Isolation | | 20 | | dB
Power CW (Average) | | 250 | | W
Power CW (Peak) | | | 500 | W
Operating Temperature Range | −10 | | +90 | °C
DRAWN M.E
CHECKED
APPROVED
SCALE CAD 1:1
MATERIAL SEE SPECIFICATION.
FINISH BODY – NICKEL PLATED
TAB – SILVER PLATED
TOLERANCES ±0.10 U.O.S.
±1/2° U.O.S.
TRAK MICROWAVE Ltd.
DUNDEE, SCOTLAND
TITLE OUTLINE DRAWING
C2425LF/J
ISSUE A B
DATE 04/08/11 10/08/11
ECN No. M.E 10513
DRG No. 896007
SHT 1 OF 1 SHTS
3
A
THE COPYRIGHT IN THIS WORK IS VESTED IN TRAK MICROWAVE LTD. AND THE DOCUMENT IS ISSUED IN CONFIDENCE FOR THE PURPOSE ONLY FOR WHICH IT IS SUPPLIED. IT MUST NOT BE REPRODUCED IN WHOLE OR IN PART OR USED FOR TENDING OR MANUFACTURING PURPOSES EXCEPT UNDER AGREEMENT OR WITH THE CONSENT IN WRITING OF TRAK MICROWAVE LTD. AND THEN ONLY ON THE CONDITION THAT THIS NOTICE IS INCLUDED IN ANY SUCH REPRODUCTION.

Dorado

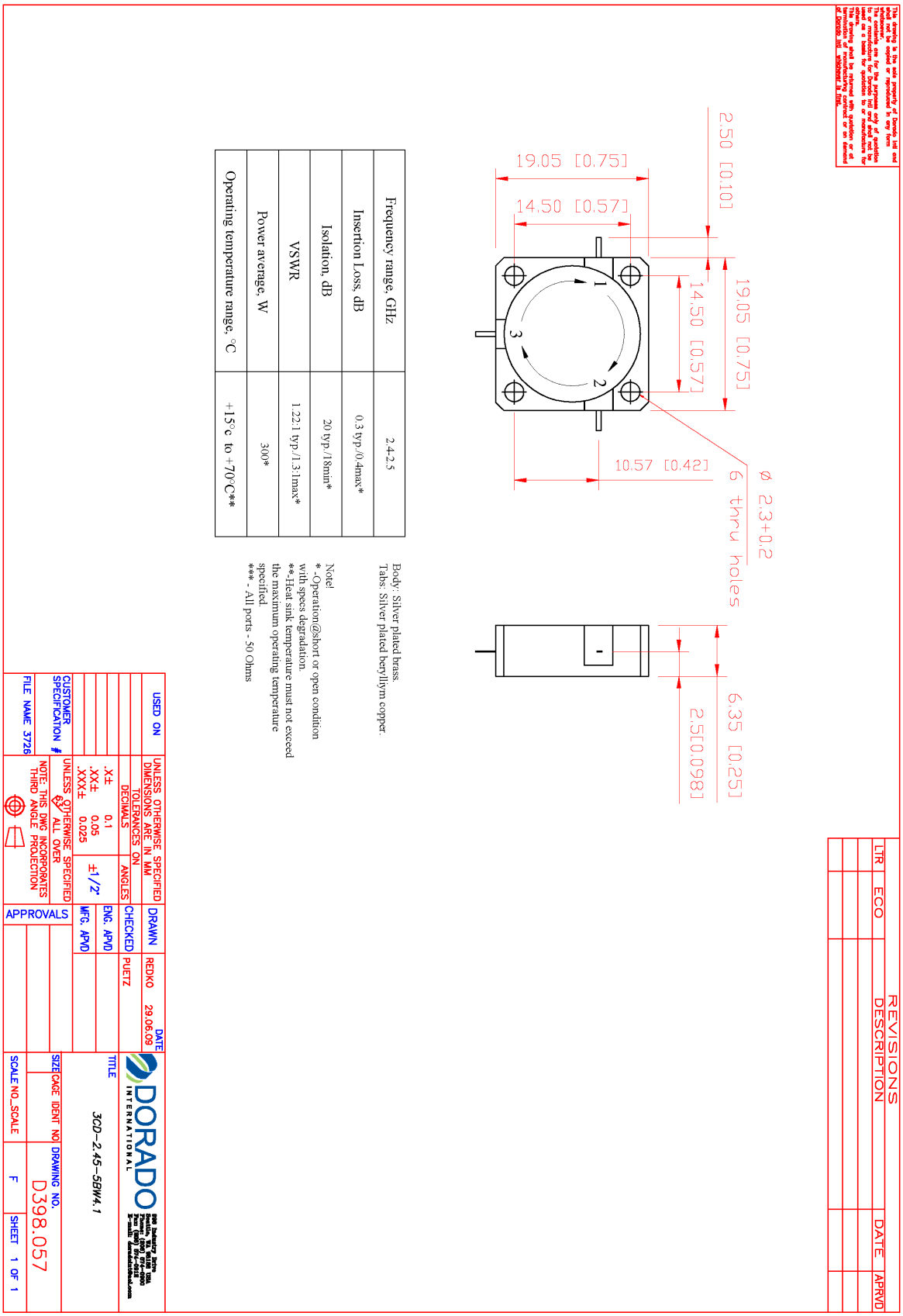

Frequency range, GHz	2.4-2.5
Insertion Loss, dB	0.3 typ./0.4max*
Isolation, dB	20 typ./18min*
VSWR	1.22:1 typ./1.3:1max*
Power average, W	300*
Operating temperature range, °C	+15°c to +70°C**

Body: Silver plated brass.
Tabs: Silver plated beryllyrn copper.

Note!
* -Operation@short or open condition with specs degradation.
**-Heat sink temperature must not exceed the maximum operating temperature specified
*** - All ports - 50 Ohms

REVISIONS

LTR	DESCRIPTION	DATE	APRVD
ECO			

DORADO INTERNATIONAL

DRAWN	REDKO	29.06.09	
CHECKED	PUETZ		
ENG. APVD			
MFG. APVD			

UNLESS OTHERWISE SPECIFIED DIMENSIONS ARE IN MM
TOLERANCES ON DECIMALS: .X± 0.1, .XX± 0.05, .XXX± 0.025; ANGLES ±1/2°
UNLESS OTHERWISE SPECIFIED ALL OVER
NOTE: THIS DWG INCORPORATES THIRD ANGLE PROJECTION

APPROVALS

USED ON

CUSTOMER SPECIFICATION #

FILE NAME 3726

TITLE: 3CD-2.45-5BW4.1

SIZE F | CAGE IDENT NO | DRAWING NO. D398.057

SCALE NO_SCALE | SHEET 1 OF 1

Circulator test-fixture

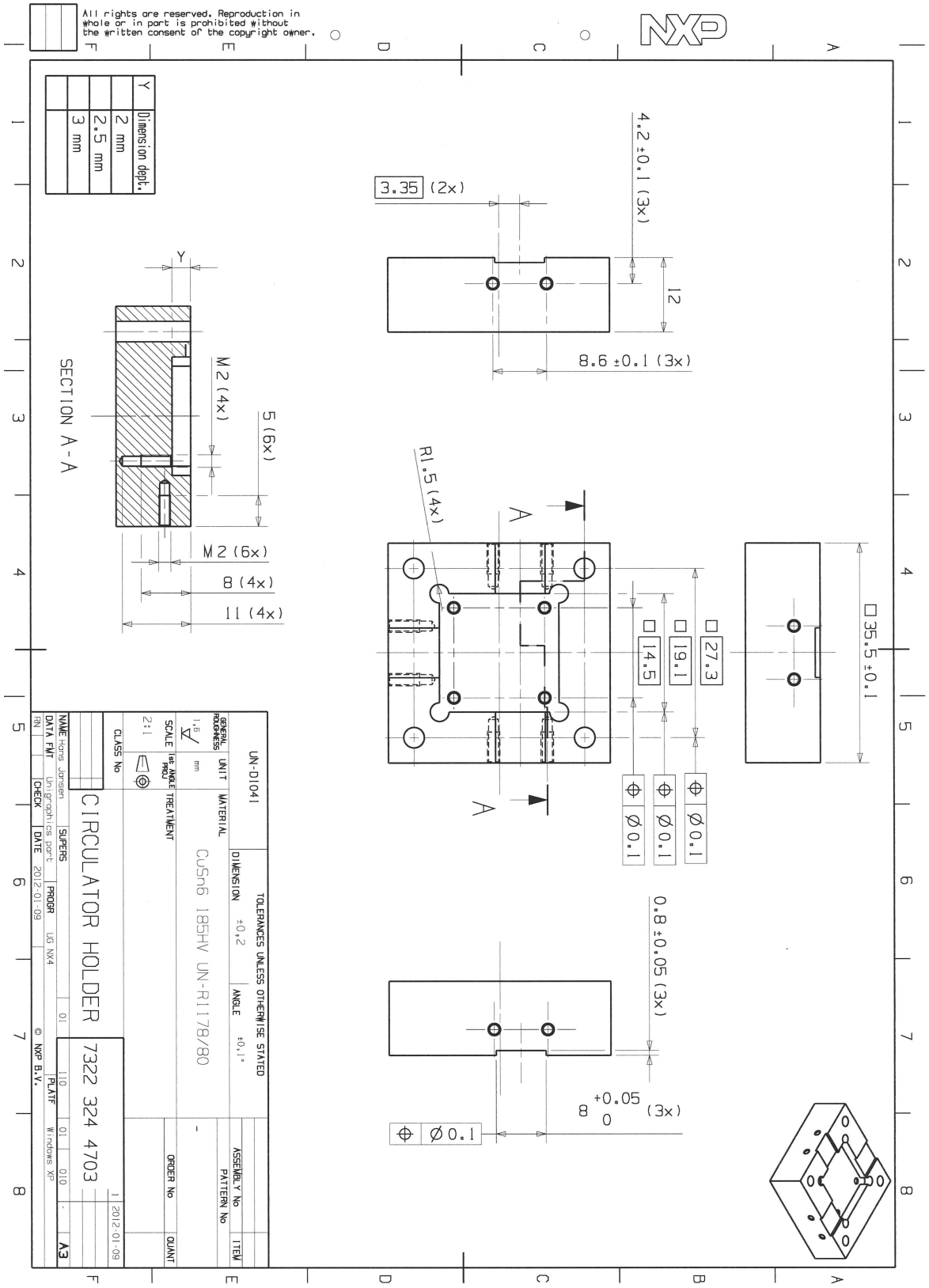

B. APPENDIX - THERMAL MEASUREMENTS

MESL test-fixture

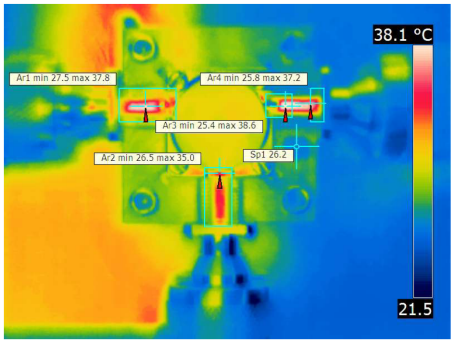

(a) $P_{in} = 50$ W, base $= 26.2$ °C , lead $= 38.6$ °C , connector $= 37.2$ °C

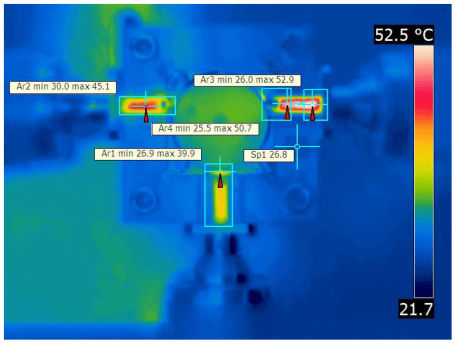

(b) $P_{in} = 75$ W, base $= 26.8$ °C , lead $= 50.7$ °C , connector $= 52.9$ °C

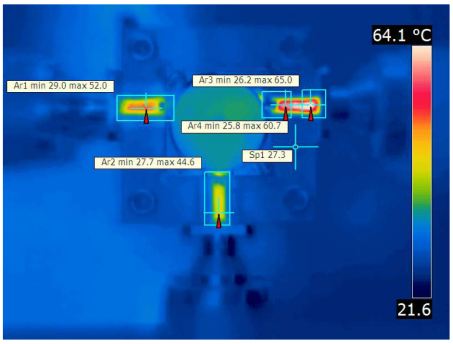

(c) $P_{in} = 100$ W, base $= 27.3$ °C , lead $= 60.7$ °C , connector $= 65.0$ °C

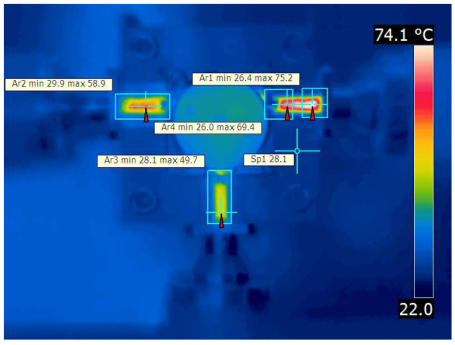

(d) $P_{in} = 125$ W, base $= 28.1$ °C , lead $= 69.4$ °C , connector $= 75.2$ °C

(e) $P_{in} = 150$ W, base $= 28.9$ °C , lead $= 78.9$ °C , connector $= 85.4$ °C

Figure B.1: MESL ruggedness test - Open circuit condition

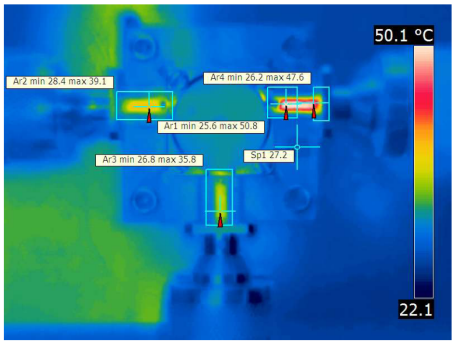

(a) $P_{in} = 50$ W, base = 27.2 °C , lead = 50.8 °C , connector = 47.6 °C

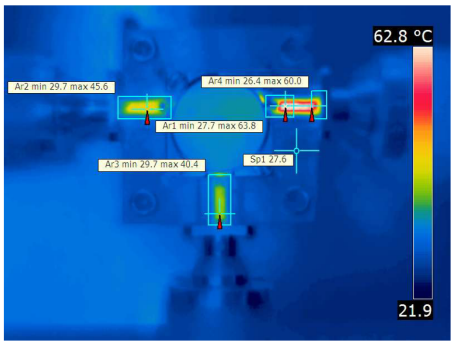

(b) $P_{in} = 75$ W, base = 27.6 °C , lead = 63.8 °C , connector = 60.0 °C

(c) $P_{in} = 100$ W, base = 28.1 °C , lead = 76.6 °C , connector = 72.7 °C

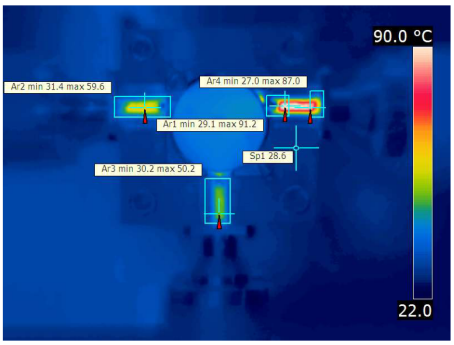

(d) $P_{in} = 125$ W, base = 28.6 °C , lead = 91.2 °C , connector = 87.0 °C

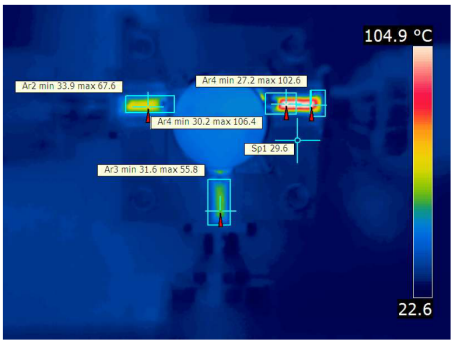

(e) $P_{in} = 150$ W, base = 29.6 °C , lead = 106.4 °C , connector = 102.6 °C

Figure B.2: MESL ruggedness test - Short circuit condition

Partron test-fixture

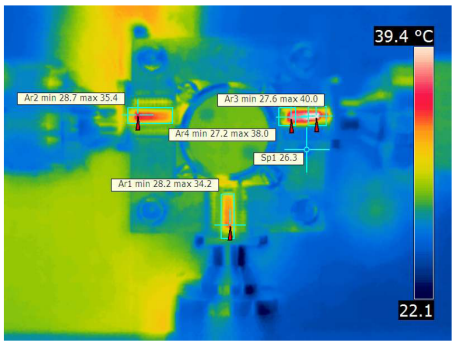

(a) $P_{in} = 50$ W, base = 26.3 °C , lead = 38.0 °C , connector = 40.0 °C

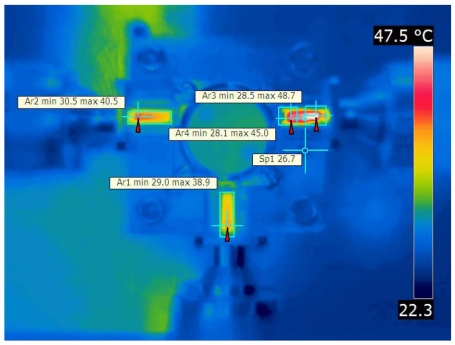

(b) $P_{in} = 75$ W, base = 26.7 °C , lead = 45.0 °C , connector = 48.7 °C

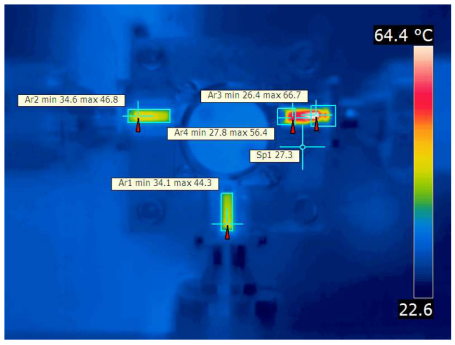

(c) $P_{in} = 100$ W, base = 27.3 °C , lead = 56.4 °C , connector = 66.7 °C

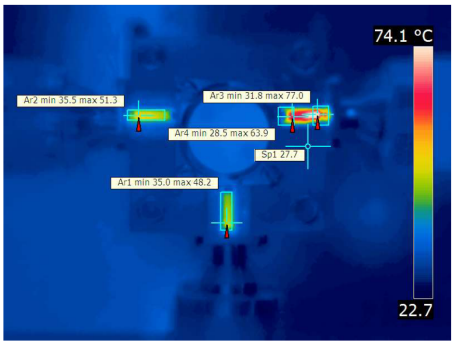

(d) $P_{in} = 125$ W, base = 27.7 °C , lead = 63.9 °C , connector = 77.0 °C

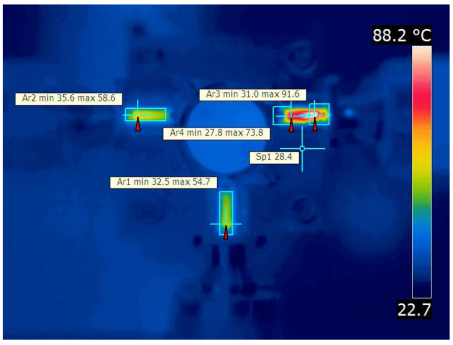

(e) $P_{in} = 150$ W, base = 28.4 °C , lead = 73.8 °C , connector = 91.6 °C

Figure B.3: Partron ruggedness test - Open circuit condition

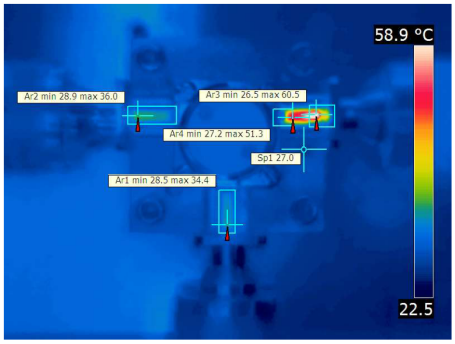

(a) $P_{in} = 50$ W, base = 27.0 °C , lead = 51.3 °C , connector = 60.5 °C

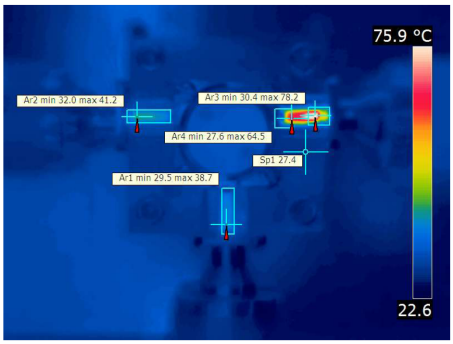

(b) $P_{in} = 75$ W, base = 27.4 °C , lead = 64.5 °C , connector = 78.2 °C

(c) $P_{in} = 100$ W, base = 28.1 °C , lead = 78.0 °C , connector = 98.1 °C

(d) $P_{in} = 125$ W, base = 28.5 °C , lead = 91.5 °C , connector = 115.6 °C

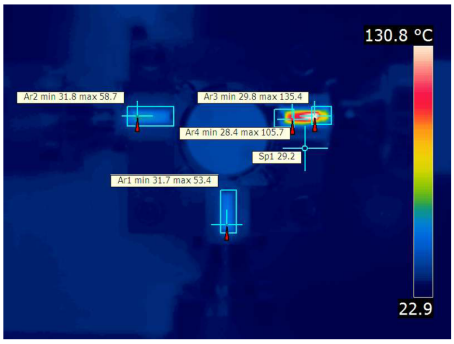

(e) $P_{in} = 150$ W, base = 29.2 °C , lead = 105.7 °C , connector = 135.4 °C

Figure B.4: Partron ruggedness test - Short circuit condition

TRAK test-fixture

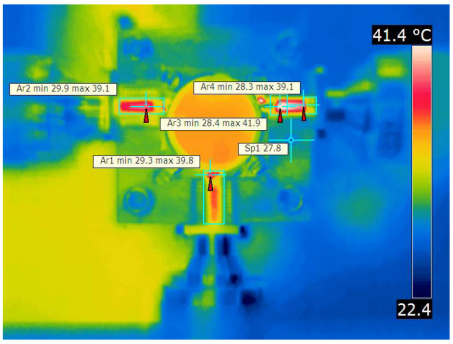

(a) $P_{in} = 50$ W, base = 27.8 °C , lead = 41.9 °C , connector = 39.1 °C

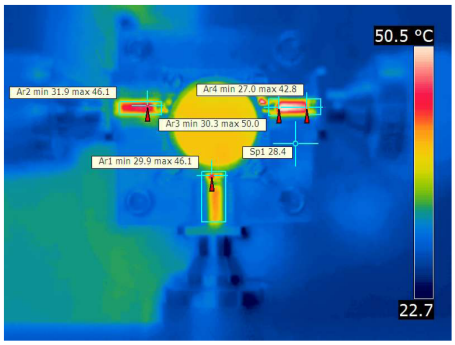

(b) $P_{in} = 75$ W, base = 28.4 °C , lead = 50.0 °C , connector = 42.8 °C

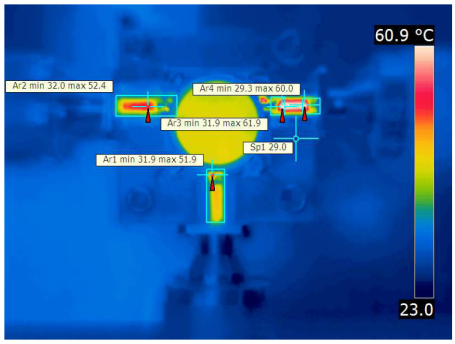

(c) $P_{in} = 100$ W, base = 29.0 °C , lead = 61.9 °C , connector = 60.0 °C

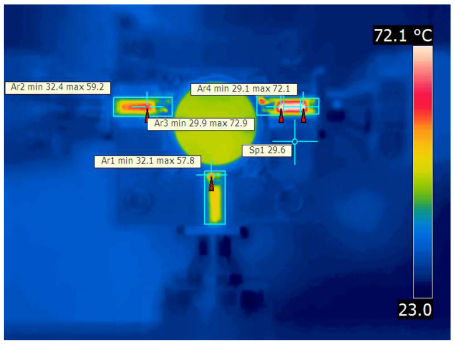

(d) $P_{in} = 125$ W, base = 29.6 °C , lead = 72.9 °C , connector = 72.1 °C

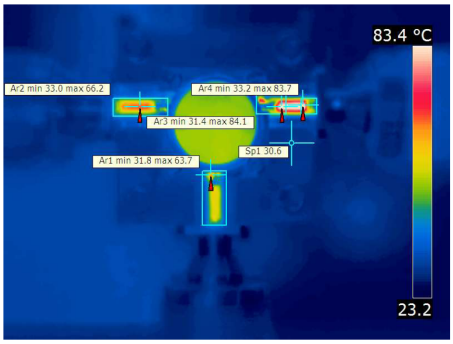

(e) $P_{in} = 150$ W, base = 30.6 °C , lead = 84.1 °C , connector = 83.7 °C

Figure B.5: TRAK ruggedness test - Open circuit condition

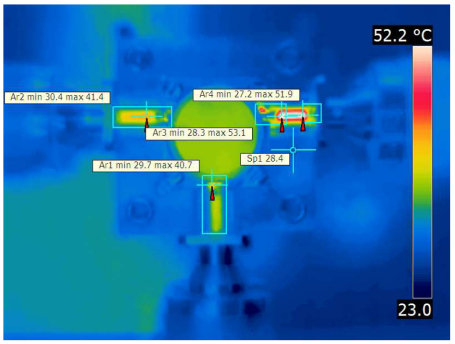

(a) $P_{in} = 50$ W, base = 28.4 °C , lead = 53.1 °C , connector = 51.9 °C

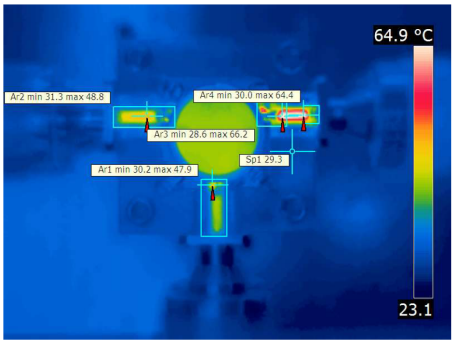

(b) $P_{in} = 75$ W, base = 29.3 °C , lead = 66.2 °C , connector = 64.4 °C

(c) $P_{in} = 100$ W, base = 30.2 °C , lead = 79.0 °C , connector = 76.5 °C

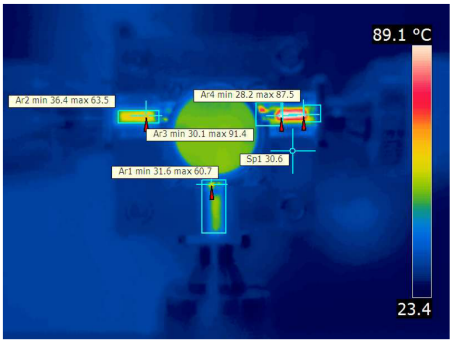

(d) $P_{in} = 125$ W, base = 30.6 °C , lead = 91.4 °C , connector = 87.5 °C

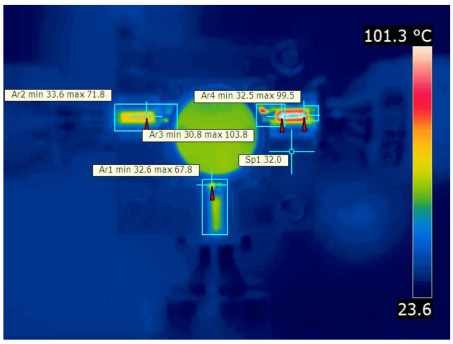

(e) $P_{in} = 150$ W, base = 32.0 °C , lead = 103.8 °C , connector = 99.5 °C

Figure B.6: TRAK ruggedness test - Short circuit condition

Renaissance test-fixture

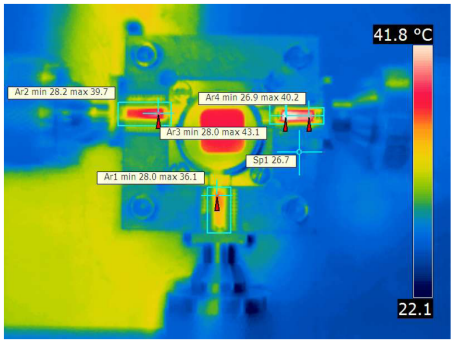

(a) $P_{in} = 50$ W, base = 26.7 °C , lead = 43.1 °C , connector = 40.2 °C

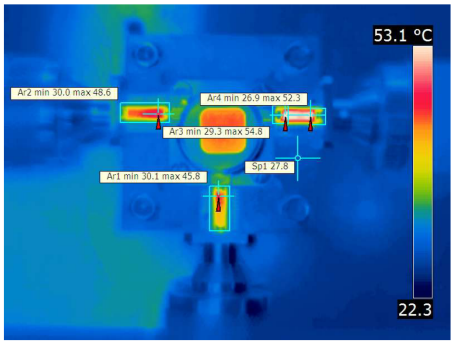

(b) $P_{in} = 75$ W, base = 27.8 °C , lead = 54.8 °C , connector = 52.3 °C

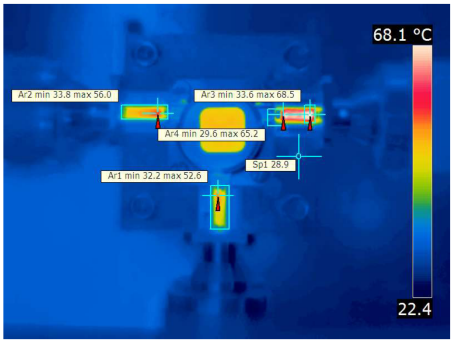

(c) $P_{in} = 100$ W, base = 28.9 °C , lead = 65.2 °C , connector = 68.5 °C

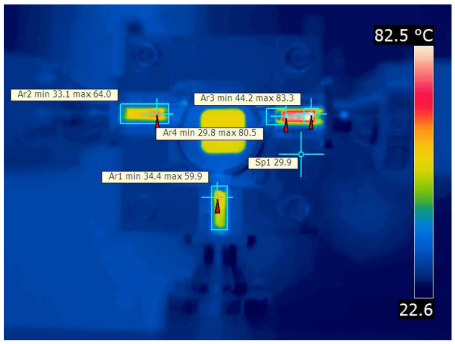

(d) $P_{in} = 125$ W, base = 29.9 °C , lead = 80.5 °C , connector = 83.3 °C

(e) $P_{in} = 150$ W, base = 31.4 °C , lead = 93.4 °C , connector = 97.4 °C

Figure B.7: Renaissance ruggedness test - Open circuit condition

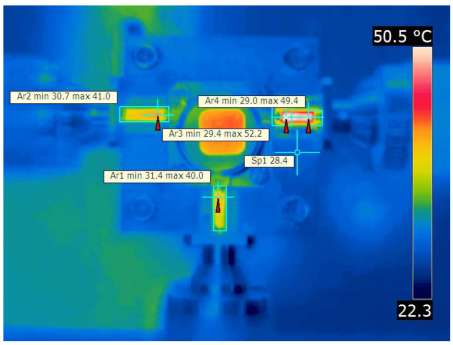

(a) $P_{in} = 50$ W, base = 28.4 °C , lead = 52.2 °C , connector = 49.4 °C

(b) $P_{in} = 75$ W, base = 29.4 °C , lead = 65.4 °C , connector = 60.8 °C

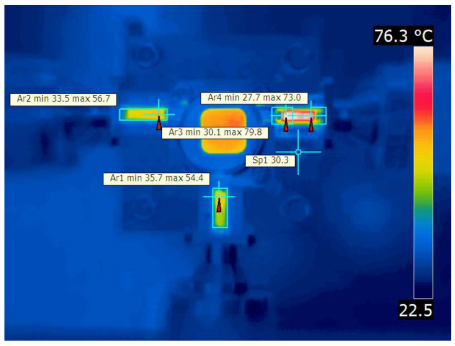

(c) $P_{in} = 100$ W, base = 30.3 °C , lead = 79.8 °C , connector = 73.0 °C

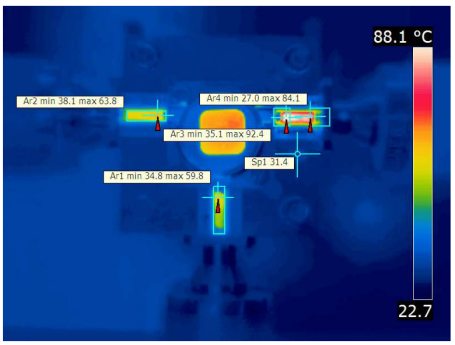

(d) $P_{in} = 125$ W, base = 31.4 °C , lead = 92.4 °C , connector = 84.1 °C

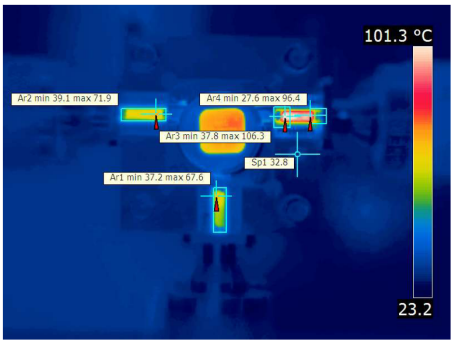

(e) $P_{in} = 150$ W, base = 32.8 °C , lead = 106.3 °C , connector = 96.4 °C

Figure B.8: Renaissance ruggedness test - Short circuit condition

Dorado test-fixture

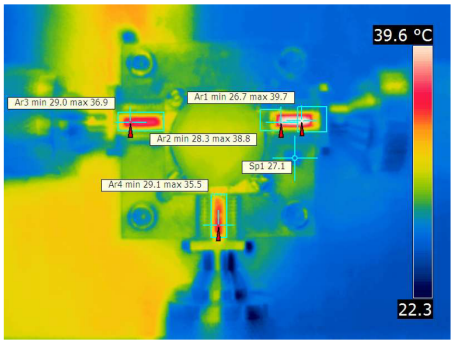

(a) $P_{in} = 50$ W, base = 27.1 °C , lead = 38.8 °C , connector = 39.7 °C

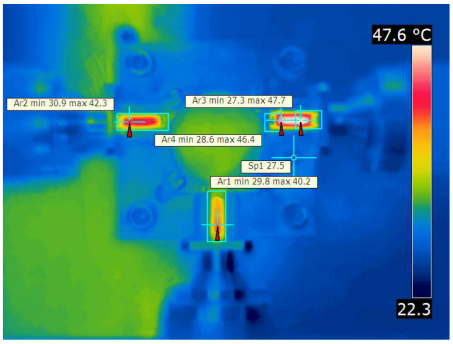

(b) $P_{in} = 75$ W, base = 27.5 °C , lead = 46.4 °C , connector = 47.7 °C

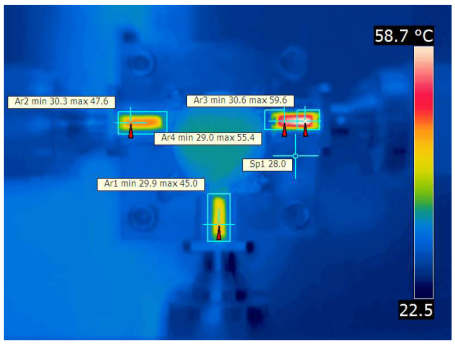

(c) $P_{in} = 100$ W, base = 28.0 °C , lead = 55.4 °C , connector = 59.6 °C

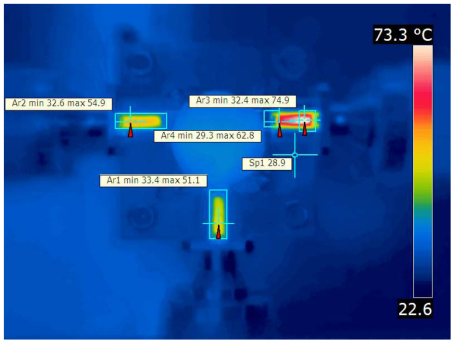

(d) $P_{in} = 125$ W, base = 28.9 °C , lead = 62.8 °C , connector = 74.9 °C

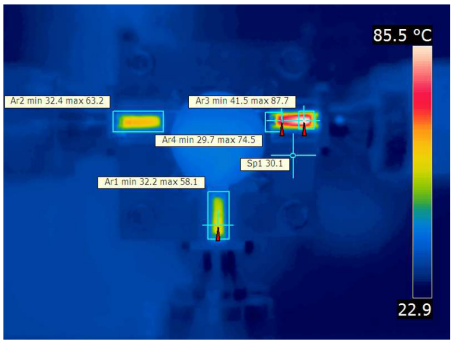

(e) $P_{in} = 150$ W, base = 30.1 °C , lead = 74.5 °C , connector = 87.7 °C

Figure B.9: Dorado ruggedness test - Open circuit condition

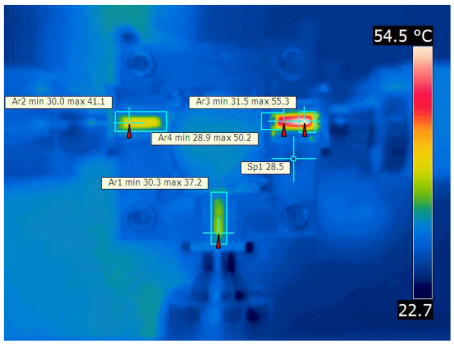

(a) $P_{in} = 50$ W, base = 28.5 °C , lead = 50.2 °C , connector = 55.3 °C

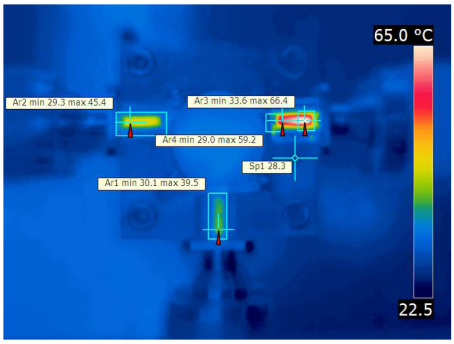

(b) $P_{in} = 75$ W, base = 28.3 °C , lead = 59.2 °C , connector = 66.4 °C

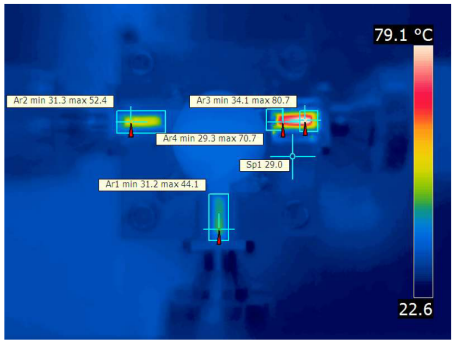

(c) $P_{in} = 100$ W, base = 29.0 °C , lead = 70.7 °C , connector = 80.7 °C

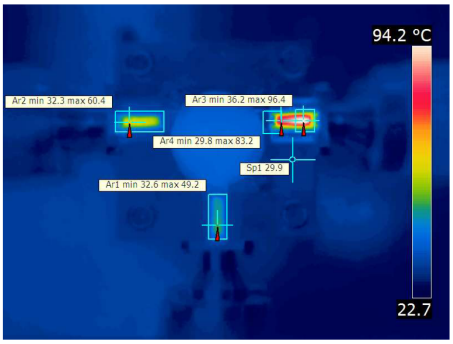

(d) $P_{in} = 125$ W, base = 29.9 °C , lead = 83.2 °C , connector = 96.4 °C

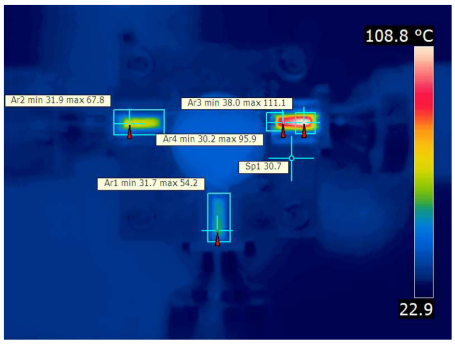

(e) $P_{in} = 150$ W, base = 30.7 °C , lead = 95.5 °C , connector = 111.1 °C

Figure B.10: Dorado ruggedness test - Short circuit condition